

Localization with random time-periodic quantum circuits

Christoph S underhauf,¹ David P erez-Garc a,^{2,3} David A. Huse,⁴ Norbert Schuch,¹ and J. Ignacio Cirac¹

¹*Max-Planck-Institut f ur Quantenoptik, Hans-Kopfermann-Str. 1, 85748 Garching, Germany*

²*Departamento de An alisis Matem atico, Universidad Complutense de Madrid, Plaza de Ciencias 3, 28040 Madrid, Spain*

³*ICMAT, Nicolas Cabrera, Campus de Cantoblanco, 28049 Madrid, Spain*

⁴*Physics Department, Princeton University, Princeton, New Jersey 08544, USA*

(Dated: October 31, 2018)

We consider a random time evolution operator composed of a circuit of random unitaries coupling even and odd neighboring spins on a chain in turn. In spirit of Floquet evolution, the circuit is time-periodic; each timestep is repeated with the same random instances. We obtain analytical results for arbitrary local Hilbert space dimension d : On a single site, average time evolution acts as a depolarising channel. In the spin $1/2$ ($d = 2$) case, this is further quantified numerically. For that, we develop a new numerical method that reduces complexity by an exponential factor. Haar-distributed unitaries lead to full depolarization after many timesteps, i.e. local thermalization. A unitary probability distribution with tunable coupling strength allows us to observe a many-body localization transition. In addition to a spin chain under a unitary circuit, we consider the analogous problem with Gaussian circuits. We can make stronger statements about the entire covariance matrix instead of single sites only, and find that the dynamics is localising. For a random time evolution operator homogeneous in space, however, the system delocalizes.

CONTENTS

I. Introduction	1	C. Spins: Simplification for numerical calculations	16
II. Settings & Questions	2	References	16
A. Gaussian circuits	3		
B. Spins	4		
III. Results	4		
A. Gaussian circuits	4		
1. Inhomogeneous evolution exhibits localization	4		
2. Homogeneous evolution delocalizes	5		
B. Spins	5		
1. Depolarising channel on each site	5		
2. Haar-distributed unitaries thermalize	6		
3. Tunable coupling strength and MBL transition	6		
IV. Proofs	7		
A. Twirling technique	7		
B. Gaussian circuits: Inhomogeneous evolution	8		
1. Haar measure on orthogonal group	8		
2. Haar measure on special orthogonal group	9		
C. Gaussian circuits: Homogeneous evolution	9		
1. Homogeneous evolution — Eigenvector delocalization	11		
D. Spins	12		
V. Numerical method for spins	13		
VI. Conclusion and Outlook	14		
Acknowledgments	15		
A. Gaussian circuits: Uncoupled case	15		
B. Spins: Uncoupled case	15		

I. INTRODUCTION

The dynamics of many-body quantum systems has received the interest in thermalization and localization. In closed systems, there are states that do not thermalize. A simple example is a single particle in a random potential that is Anderson localized [1]. But even if one includes interactions, a new way of many-body localization (MBL) can emerge that also prevents thermalization [2]. Despite great progress in understanding MBL during the last years (see eg. [3] or the review [4]), there are still many open questions.

A typical scenario studied in the context of localization is a system on a one-dimensional lattice, with a short-ranged Hamiltonian containing a kinetic term and a random potential for each site. In the absence of interactions, this single-particle problem displays Anderson localization: Starting in one position, the probability of finding the particle at the same position after arbitrary time is lower bounded, and the probability for other positions is exponentially suppressed [5, 6]. If one adds interactions, the system can find itself in the thermal or MBL phase, usually dependent on disorder strength. Starting with some information in a specific position, in the thermal phase it will flow away and cannot be recovered locally, and in the MBL phase there will still be traces present at the same position after arbitrarily long times, despite some information slowly flowing away [7–9].

Another scenario is so-called Floquet evolution. There, one considers not continuous time evolution generated by time-invariant Hamiltonians, but a discrete-time evolution operator repeated for subsequent timesteps. It may

arise from a periodic drive or be directly given as a unitary model. Floquet systems are a formidable setting to study localization, because even energy ceases to be a conserved quantity. Anderson localization has been proven for specific Floquet systems [10]. It has been found that Floquet systems are compelling examples for MBL [11, 12] which yield sharper transitions between thermal and MBL phases [13].

In addition, circuits of random unitaries have recently been used as a model of chaotic systems [14–22]. In [14, 17], time evolution by a unitary circuit of fixed geometry but independently Haar-distributed random gates at each time step was studied. That model exhibits thermalization to an infinite temperature state, and the authors found ballistic spreading of quantum information by considering the out-of-time-ordered correlator. Subsequently the model was extended to a similar setup [15, 18] with a conservation law. In [16], the authors consider the same unitary circuit in a Floquet setting, where subsequent timesteps are repeated with the same random instances. In the limit of infinite local Hilbert space dimension for each qudit, they find thermalization to an infinite temperature state and calculate several values like the spectral form factor or the exponentials of some Renyi-entropies. In other related work [23–25], thermalization of spin chains for certain continuous-time dynamics was found in the context of the average spectral form factor.

Here, we consider several variations of Floquet evolution with a unitary circuit, and analyse if there is localization. We consider as time evolution operator a quantum circuit of depth two, which consists of two alternating layers of random nearest-neighbor unitaries coupling even and odd pairs of sites in turn. The two layers are repeated identically for subsequent timesteps such that the total circuit is periodic in time, in the spirit of Floquet evolution. This circuit geometry is the discrete analogue of local time-independent Hamiltonian evolution (and could also be obtained by a Trotter decomposition, or the standard form of an index zero matrix product unitary [48], for example). We perform an average within a (sub)set of unitaries. Typically, we start with a completely mixed state everywhere and a pure state at one site and look at the reduced state of that and other sites at some later time, and determine whether it depends on the initial state, corresponding to localization.

The scenarios we consider are the following: (A) Gaussian circuits, acting on fermionic chains with one mode per site and Gaussian evolution, where the nearest-neighbor unitaries in the circuit are operations that stay within the manifold of fermionic Gaussian states. (B) Spins, with a qudit per site and arbitrary constituent unitaries in the circuit. The first scenario, (A) Gaussian circuits, extends the typical situation in Anderson localization, since particle number is not conserved. In this scenario, we consider inhomogeneous as well as homogeneous Floquet circuits, where the unitaries coupling sites are independently random for each pair of neighbors or the same along the entire chain. We find that the in-

homogeneous setting exhibits localization, whereas the homogeneous Floquet circuit leads to delocalization.

The second scenario, (B) spins, is similar to the models studied in [14, 16, 17]. In contrast to [16], in our work the local Hilbert space dimension of each spin is finite, and in contrast to [14, 17], we work in a Floquet setting. We prove that on a single site, the time evolution acts as a depolarising channel. Further, we find that a chain of qubits can exhibit thermalization or MBL, depending on the probability distribution used to average the unitaries in the circuit; we observe the corresponding phase transition.

Our setup is difficult computationally and analytically, because it requires to study dynamics of many-body systems, averaged over instances of the random Floquet circuit. Methods to exactly calculate averages [26, 27] work well when each random matrix appears a small amount of times, or for large dimensions where asymptotic behaviour is available. These methods are not useful in our setting, since the same random matrices reappear in each timestep (contrary to [14, 17]) and we have a fixed finite dimension of the spins (contrary to [16]). Instead, we derive analytical results in both cases with a technique we call the twirling technique. It is based on a property of the average, which basically allows us to move arbitrary single-site unitaries through the quantum circuit such that they only appear twice, at the beginning and end, relating initial and final states.

Apart from that, we also perform numerical calculations [47] in both cases. For (A) Gaussian circuits, we can work with the covariance matrix formalism, which is very efficient and allows us to explore very large systems. For (B) spins, the Hilbert space is exponential in chain length. We develop a new numerical method which combines tensor networks and Monte Carlo ideas, drawing from simplifications provided by the analytic results. It reduces the memory and time complexity from 2^{4t} to 2^t for t timesteps. This allows us to study relatively long times which, in turn, enables the simulation of up to 39 spins.

This article is organized as follows. First, we introduce the precise models in section II and the quantities we will compute. In section III we present the main results of this work, and leave the derivations for section IV. There, we also present the twirling technique (section IV A) used throughout the paper, which can also be of interest on its own. Finally, in section V we present the new numerical method used for spin chains.

II. SETTINGS & QUESTIONS

For a one-dimensional chain of N particles, we consider a random unitary time evolution operator U composed of random nearest-neighbor gates according to some probability distribution. The time evolution operator is the unitary circuit with the fixed geometry sketched in Fig. 1

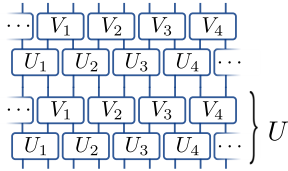


FIG. 1. Random time evolution operator U^2 for two timesteps. The vertical lines indicate sites of the chain; each unitary couples two neighboring sites. In the spirit of Floquet evolution, the total evolution operator is time-periodic; the time step is repeated with the same random instances of U_i, V_i .

and can be written as

$$U = \left(\bigotimes_i V_i \right) \left(\bigotimes_i U_i \right). \quad (1)$$

The unitary U_i acts on particles $2i - 1$ and $2i$ while V_i acts on sites $2i$ and $2i + 1$. These two layers are repeated identically (with the same random instances of U_i, V_i) in spirit of Floquet evolution, in contrast to other models [14, 17] where each timestep is different.

In this article, we study the random circuit as a time evolution operator that is a (A) Gaussian circuit for fermionic chains or (B) Unitary circuit for spin chains. Throughout, the average $\langle \cdot \rangle$ denotes averaging over U_i, V_i . In the next two subsections, we give details of both settings, and define the probability distributions used for the average $\langle \cdot \rangle$ in either setting.

A. Gaussian circuits

First, we consider the problem for a chain of fermionic systems with one fermionic mode per site. Each of the N modes has two Majorana operators

$$c_{2n-1} = a_n^\dagger + a_n, \quad c_{2n} = -i(a_n^\dagger - a_n), \quad (2)$$

with the creation/annihilation operators a_n^\dagger/a_n . The two-point correlation functions of Majorana operators for each fermionic state ρ can be gathered in the covariance matrix

$$\Gamma_{kl} := \frac{i}{2} \text{Tr}(\rho[c_k, c_l]). \quad (3)$$

Each site of the chain corresponds to a 2×2 block because each site is associated with two Majorana operators. A fermionic Gaussian state (i.e. those that can be generated by the vacuum of a_n by Gaussian functions of the Majorana operators) is completely and uniquely characterized by its covariance matrix. Here, we consider the covariance matrices of not only Gaussian but arbitrary initial states with vanishing two-point correlators at non-zero distances.

We build the Gaussian circuit of transformations that map Gaussian states to Gaussian states (but can still be

applied to general states). The most general such unitary operation acts on the covariance matrix by an orthogonal transformation $O \in O(2N)$, specifically $\Gamma \rightarrow O\Gamma O^T$.

We will consider two classes of these unitary transformations: Gaussian operations generated by Hamiltonians quadratic in the Majorana operators, which correspond to special orthogonal transformations $O \in SO(2N)$ in the covariance matrix formalism [28, 29], and the larger class of all operations $O \in O(2N)$ which includes local particle-hole transformations [30]. Subsequently, we only consider the covariance matrices of initial and final states.

In this setup, the unitary-circuit time evolution operator (1) is represented as an orthogonal transformation $O \in O(2N)$ built of random two-site operations $P_i, Q_i \in O(4)$. With periodic boundary conditions,

$$O = G \left(\bigoplus_{i=1}^{N/2} Q_i \right) G^T \left(\bigoplus_{i=1}^{N/2} P_i \right), \quad (4)$$

where

$$G = \begin{pmatrix} 0 & & & \mathbb{I}_2 \\ \mathbb{I}_2 & 0 & & \\ & \ddots & \ddots & \\ & & \mathbb{I}_2 & 0 \end{pmatrix} \quad (5)$$

takes care of circularly shifting $\bigoplus Q_i$ by one site; i.e. two matrix elements down and right. Thereby P_i couples site $2i - 1$ with $2i$ and Q_i couples site $2i$ with $2i + 1$.

Our quantity of interest is the average final state $\langle \Gamma_t \rangle$ after t timesteps of an initially uncorrelated product state Γ_0 , i.e. with a 2×2 block-diagonal covariance matrix. In this formalism its covariance matrix is

$$\langle \Gamma_t \rangle = \langle O^t \Gamma_0 O^{t\dagger} \rangle. \quad (6)$$

For the expectation value $\langle \cdot \rangle$, we consider two probability measures for the P_i, Q_i : the Haar measure for the orthogonal group $P_i, Q_i \in O(4)$ and the Haar measure for the special orthogonal group $P_i, Q_i \in SO(4)$. The Haar distribution (see eg. [31]) for the orthogonal (special orthogonal) group $O(4)$ ($SO(4)$) is defined as the unique distribution with the property of Haar invariance, which mandates that any transformation

$$P \rightarrow APB, \quad \text{for any } A, B \in O(4) \text{ } (SO(4)) \quad (7)$$

does not affect averages $\langle \cdot \rangle$ with respect to $P \in O(4)$ ($SO(4)$) [32]. The long-time behaviour of an initial covariance matrix is readily accessible to numerical calculations even on long chains, because we need only operate on its covariance matrix, whose dimension grows merely linearly in system size.

We consider two scenarios. In the first scenario, all P_i, Q_i are independently distributed according to one of the Haar measures. This situation is related but not equivalent to that studied in context of Anderson localization. The main reason is that the average over

O includes transformations P_i, Q_i that do not conserve particle number. Thus, a question to be addressed is whether the well-studied phenomenon of Anderson localization still exists, or if it is modified. To this end we ask, does the average final state $\langle \Gamma_t \rangle$ contain remnant information about the initial state Γ_0 ? The corresponding results are reported in section III A 1.

Furthermore, we study a second scenario, the homogeneous setting where the time evolution operator O is 2-site-translation invariant. In that scenario, randomness is the same for all sites, $P_i = P_j$ and $Q_i = Q_j$, such that there are only two independent transformations; here we consider only the Haar measure over $O(4)$. Again, we ask the same question: Does an impurity in an otherwise translation-invariant state spread all over the chain or stay localized? We present the answer in section III A 2. Occasionally, the time average

$$\langle \Gamma_{t\text{-avg}} \rangle := \lim_{T \rightarrow \infty} \frac{1}{T} \sum_{t=0}^{T-1} \langle \Gamma_t \rangle \quad (8)$$

is used to assess the localising or delocalising properties. Physically, it captures the long-time behaviour of a typical state. The additional average allows us to make stronger statements.

B. Spins

After studying the evolution of a chain of fermions under Gaussian circuits, we turn to a chain of interacting spins. All particles along the chain have a local Hilbert space dimension d , which may be arbitrary. In that setting, all of the unitaries U_i, V_i composing the circuit U are general unitaries of $U(d^2)$, independently distributed according to some probability distribution for the average $\langle \cdot \rangle$.

We will consider different probability distributions for $U_i, V_i \in U(d^2)$ with the common property of single-site Haar invariance. This means that any transformation of a U_i or V_i of the form

$$U_i \leftrightarrow (w_1 \otimes w_2) U_i (w_3 \otimes w_4) \quad (9)$$

does not affect averages $\langle \cdot \rangle$, for arbitrary choice of $w_j \in U(d)$. For example, the unitary Haar distribution on $U(d^2)$ has this property. It is a distribution uniquely defined by Haar invariance (see eg. [31]), which means that transformations of the form $U \rightarrow AUB$, for arbitrary $A, B \in U(d^2)$, do not affect any averages with respect to the Haar distribution of $U \in U(d^2)$ [32].

In this article, we characterize the average final state $\langle \rho_t \rangle$ obtained from an initial density matrix ρ_0 after t timesteps:

$$\langle \rho_t \rangle := \langle U^t \rho_0 U^{t\dagger} \rangle. \quad (10)$$

In particular, for arbitrary initial states ρ_0 , we will find a relation between the reduced initial state $\rho_0^{\text{red}} :=$

$\text{Tr}_{\{1\dots N\} \setminus \{n\}} \rho_0$ on a single site n and the reduced state $\langle \rho_t^{\text{red}} \rangle := \text{Tr}_{\{1\dots N\} \setminus \{n\}} \langle \rho_t \rangle$ of the average final state on the same site. We find that on a single site, average time evolution acts as a depolarising channel. This result is formulated in section III B 1.

With this local characterization of initial and average final states, we assess the long-time behaviour of $\langle \rho_t^{\text{red}} \rangle$ numerically. Interacting systems may thermalize, or else display many-body localization. In this context, we ask, does $\langle \rho_t \rangle$ locally remember the initial state (localization) or not (thermalization)? For example, imagine an initial state that is homogeneous except for an impurity at one site. Then we ask, after average time evolution, can we perform local measurements at the same or other sites to recover information about the position and initial state of this impurity? We present our corresponding results in sections III B 2 and III B 3.

III. RESULTS

In this section, we present our main results for (A) Gaussian circuits or (B) spins. We leave the details of the derivations, as well as the methods used to obtain them, for the next sections.

A. Gaussian circuits

First, we consider the setting of Gaussian circuits. We will first consider the inhomogeneous case, where orthogonal matrices for different sites are independently random. Then we will give the results for the homogeneous case, where the time evolution operator is invariant under translations by two sites.

1. Inhomogeneous evolution exhibits localization

For uncorrelated initial states Γ_0 , i.e. 2×2 block-diagonal Γ_0 , we find the following result:

$$\langle \Gamma_t \rangle = c(t, N) \Gamma_0. \quad (11)$$

The constant $c(t, N)$ is independent of the initial state. We obtain this result for both the orthogonal Haar measure, $P_i, Q_i \in O(4)$, as well as the special orthogonal Haar measure, $P_i, Q_i \in SO(4)$, with the same constant $c(t, N)$ in both cases. The latter case holds as long as $t < (N - 1)/2$, i.e. the system is large enough to accommodate the lightcone without self-intersections. Hence in the thermodynamic limit, $O(4)$ and $SO(4)$ Haar averages are equivalent in this setting. We prove these results in section IV B.

We further study $c(t, N)$ numerically, and plot it in Fig. 2 as a function of time steps t for different system sizes N . We observe that $c(t, N)$ converges to a fixed value $c \approx 0.06$, irrespective of N . After one time step,

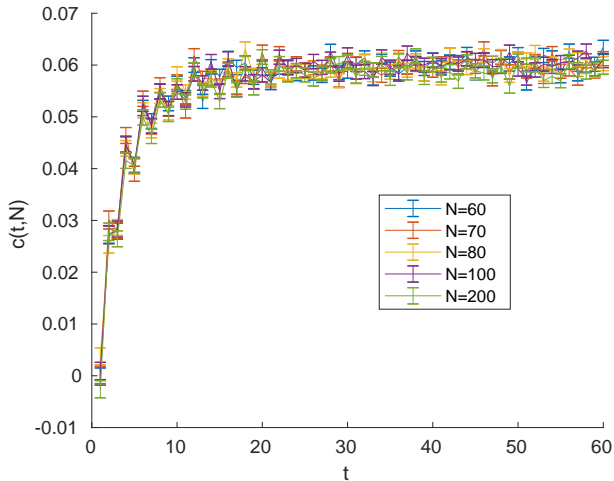


FIG. 2. The constant $c(t, N)$ with which a fermionic covariance matrix is scaled by random time evolution for t timesteps, see eq. (11). We generate 10^4 samples of $O(4)$ -Haar-distributed $P_i, Q_i \in O(4)$ for each data point. Surprisingly, $c(t, N)$ does not depend on system size N even for t large enough such that the lightcone wraps around the periodic boundaries.

$c(1, N) = 0$ exactly, which simply is thermalizing evolution with independent Haar distributed orthogonals. Only at longer times does the time-periodic structure of the circuit become manifest and result in appreciably change in measure. Since $c(t, N)$ reaches a non-zero value, we find that Anderson localization still happens in this extended setup; an initially localized impurity stays localized. Each site of the initial state is simply scaled towards the thermal mixture $\Gamma = 0$ by the same factor $c(t, N)$. Nevertheless, after average time evolution, the initial state's covariance matrix can still be fully reconstructed from measured expectation values, albeit their variances increase.

2. Homogeneous evolution delocalizes

Next, let us consider a homogeneous time evolution operator, where $P_i = P_j \in O(4)$ and $Q_i = Q_j \in O(4)$ are distributed according to the orthogonal Haar measure. Let Γ_0^n be an initial state with a single site n occupied and all others maximally mixed. This is a zero matrix, except that the 2×2 block for site n is $\gamma := \begin{pmatrix} 0 & 1 \\ -1 & 0 \end{pmatrix}$. In section IV C we show the time-averaged final state of this initially localized state to have the covariance matrix

$$\langle \Gamma_{t\text{-avg}}^n \rangle := \lim_{T \rightarrow \infty} \frac{1}{T} \sum_{t=0}^{T-1} \langle \Gamma_t^n \rangle = \frac{1}{N/2} \Gamma_*, \quad (12)$$

under a plausible assumption about disjointness of spectra of matrices that are multiplied by Haar-random orthogonal matrices which we also verified numerically. We characterize Γ_* further in section IV C.

An important part of the result is that the covariance matrix Γ_* depends not on the precise value of n but only on $n \bmod 4$. Thus, the location n of the impurity cannot be reconstructed from $\langle \Gamma_{t\text{-avg}}^n \rangle$. Moreover, in the thermodynamic limit, the prefactor $1/(N/2)$ causes $\langle \Gamma_{t\text{-avg}}^n \rangle$ to reach the infinite temperature thermal mixture 0. In conclusion, our result implies the absence of localization.

A complementary viewpoint of delocalization is provided by the delocalization of eigenvectors of a single generic random instance of the time evolution operator. In section IV C 1 we prove how this allows us to bound all matrix elements of $\Gamma_{t\text{-avg}}^n$ for a generic evolution operator O with non-degenerate spectrum:

$$|(\Gamma_{t\text{-avg}}^n)_{ij}| \leq \frac{16}{N} \rightarrow 0 \quad (13)$$

in the thermodynamic limit, without resorting to an ensemble average $\langle \cdot \rangle$. On the one hand, this result is stronger than (12) insofar as it shows $\Gamma_{t\text{-avg}}^n \rightarrow 0$ in the thermodynamic limit already for single instances of the time evolution operator. On the other hand, it only gives a bound $\leq \frac{16}{N}$ and not an explicit form.

B. Spins

We now move from Gaussian circuits to interacting spins. The average $\langle \cdot \rangle$ is now an average over all nearest-neighbor unitaries $U_i, V_i \in U(d^2)$ comprising the time evolution operator, independently distributed according to some probability distribution with single-site Haar invariance (see II B). Here we will first present the statement that relates the evolution of a single site with a depolarising channel. Then, we show results which indicate the absence of localization when averaging with the Haar measure on $U(4)$. Finally, we will consider different unitary ensembles, which vary in the degree of entanglement the U_i, V_i generate and present numerical evidence for a thermal-MBL phase transition.

1. Depolarising channel on each site

Our first result is, that on a single site, the average time evolution (10) acts as a depolarising channel. To make this result precise, consider an arbitrary initial state ρ_0 . Split its reduced density matrix for one site

$$\rho_0^{\text{red}} = \mathbb{I}_d/d + \bar{\rho}_0^{\text{red}} \quad (14)$$

into traceful and traceless part $\bar{\rho}_0^{\text{red}}$. For the evolved reduced state at the same site we prove

$$\langle \rho_t^{\text{red}} \rangle = \mathbb{I}_d/d + \alpha(t) \bar{\rho}_0^{\text{red}}. \quad (15)$$

This corresponds to a depolarising channel [33] with depolarization probability $1 - \alpha(t)$. The real constant $\alpha(t)$ is independent of the initial state. Provided the lightcone ($2t + 1$ sites in width) around the site fits into the system,

it is also independent of the position of the site and of system size. Moreover, it is striking that the final state on a single site is affected only by the initial state on the same site, and is independent of the initial state at all other sites. We prove (15) in section IV D where we also derive a similar formula for the two-site reduced density matrix.

If the initial state is free of inter-site correlations, with all but one site completely mixed, the final state can be fully characterized. Thereby the initial state $\rho_0 = \mathbb{I}_d/d \otimes \rho_0^{\text{red}} \otimes \mathbb{I}_d/d \otimes \mathbb{I}_d/d \otimes \dots$ evolves to a final state with the same structure $\langle \rho_t \rangle = \mathbb{I}_d/d \otimes \langle \rho_t^{\text{red}} \rangle \otimes \mathbb{I}_d/d \otimes \mathbb{I}_d/d \otimes \dots$.

To understand the behaviour of the system, it is necessary to determine the behaviour of $\alpha(t)$. For this, we will study $\alpha(t)$ numerically for spin 1/2 particles, $d = 2$. In order to access long times, we use a new numerical method (section V). It reduces the complexity for t timesteps from $2^{2(2t+1)}$ to 2^t and uses an importance sampling technique to lower the variance. Since the number of spins involved after t timesteps is $2t + 1$, this in turn has allowed us to reach 39 of them while maintaining an effectively infinite system size.

2. Haar-distributed unitaries thermalize

As a concrete probability distribution for the unitaries U_i, V_i , we first consider the Haar distribution on $U(4)$. In Fig 3 we present numerical results for this probability distribution. They show that α vanishes exponentially as $t \rightarrow \infty$, with a half-life of about 1.8 timesteps. Therefore we find thermalization to a locally infinite temperature state: The map (15) describing a single site's evolution becomes completely depolarising in the limit $t \rightarrow \infty$ where $\alpha \rightarrow 0$. A similar result has been obtained in [23] in a Hamiltonian (continuous time evolution) setting.

This result is in stark contrast to the analogous setting with Gaussian circuits (section III A 1). A Floquet operator built of unitaries conserving Gaussianity as studied in that setting causes localization, while taking into account all unitaries, it causes thermalization. The reason for this difference can be attributed to the fact that MBL phases are not ubiquitous in parameter space [34], whereas Anderson localization is (in 1D models, as analysed here).

3. Tunable coupling strength and MBL transition

As seen in the previous section, the Haar distribution exhibits thermalising behaviour, since MBL can typically only be found for strong random potentials relative to the coupling [34]. In practice, Haar-distributed U_i and V_i contain many highly entangling operators which can move information that is initially contained in one site across the chain. This opens up the question of whether MBL can be found by considering less entangling operations. We therefore modify the distribution used for the unitaries composing the time evolution operator.

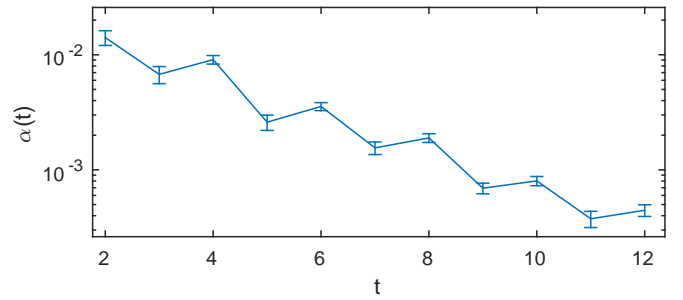


FIG. 3. The constant $\alpha(t)$ relating initial and final states (15) for Haar-distributed unitaries. The figure is indicative of thermalization at long times as α vanishes exponentially in time. For each data point, 10^3 samples of random unitaries were generated.

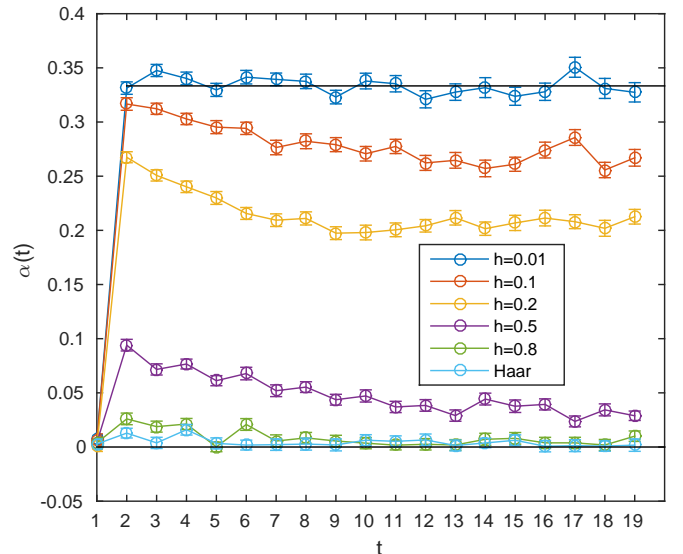


FIG. 4. The constant $\alpha(t)$ relating initial and final states (15) for unitaries distributed according to (16) with random coupling strength h . For strong coupling $\alpha(t)$ relaxes to zero and the system thermalizes. In contrast $\alpha(t)$ reaches a finite value at weak couplings and the system displays localization. Horizontal lines indicate $\alpha = 0$ and the exact decoupled value $h = 0, \alpha = 1/3$. See section V for the numerical method used.

Every unitary in $U(4)$ can be cast in the form [35]

$$(u_1 \otimes u_2) e^{ia \sigma_x \otimes \sigma_x + ib \sigma_y \otimes \sigma_y + ic \sigma_z \otimes \sigma_z} (u_3 \otimes u_4) \quad (16)$$

with $u_i \in U(2)$ and coefficients $a, b, c \in \mathbb{R}$. σ_i denote the Pauli matrices. We define a probability distribution for all $U_i, V_i \in U(4)$ composing the time evolution operator by means of this form, drawing each u_i from the Haar measure for $U(2)$ and a, b, c uniformly from the interval $[-h, h]$. Note that this distribution possesses single-site Haar invariance, so that the results of section III B 1 still apply.

In Fig. 4 we present numerical results for $\alpha(t)$ for distributions with various coupling strengths h . In the figure, we find a crossover from thermalization for large cou-

pling where $\alpha(t) \rightarrow 0$ and localization for small coupling where $\alpha(t)$ reaches a finite value and the map (15) keeps information about the initial state. In the completely uncoupled case $h = 0$, $\alpha = 1/3$ is reached exactly (appendix B), consistent with the behaviour for $h \rightarrow 0$.

The MBL transition can be extracted from $\alpha(t = \infty)$ as a function of h . Alternatively, it may be pin-pointed by considering the entanglement entropy of the time evolution operator's eigenstates in the limit of an infinite system. In the thermal phase, the eigenstates have volume law entanglement while in the MBL phase they have lower area law entanglement [36, 37]. Results obtained from exact diagonalization of small systems are shown in Fig. 5 alongside $\alpha(t = 18)$. It is interesting to consider also the variance of the different eigenstates' entanglement, also plotted in Fig. 5. Because all eigenstates have similar entanglement properties in both thermal and MBL phases, the variance peaks near the phase transition where the entanglement is intermediate between these limits in a way that varies strongly between eigenstates [38]. Those measures all agree and clearly indicate a finite-size or finite-time estimate of the MBL transition at coupling strength near $h_0 \approx 0.3$. Such estimates are known to drift systematically towards the MBL phase as the size of the system is increased [13], as can be seen from the crossings in the middle panel of Fig. 5, so the actual phase transition is most likely at a value of h smaller than this.

IV. PROOFS

In this section, we give detailed proofs for the analytic results reported above. The numerical method is explained in the section after. First, we present a technique used throughout that we call the twirling technique (section IV A). Then we show our results for Gaussian circuits, under inhomogeneous evolution in section IV B and homogeneous evolution in section IV C. In the latter case, we also explain the complementary viewpoint provided by eigenvector delocalization. Finally, we proof the results for spin chains in section IV D.

A. Twirling technique

In this section, we present a technique we call twirling technique, which recurs in the proofs of our results. The idea is to exploit single-site Haar invariance of the probability distribution for the unitaries. Single-site Haar invariance means that any transformation of a U_i or V_i of the form

$$U_i \leftrightarrow (w_1 \otimes w_2)U_i(w_3 \otimes w_4) \quad (17)$$

does not affect averages $\langle \cdot \rangle$, for arbitrary choice of $w_j \in U(d)$.

Our procedure is depicted in Fig. 6. At any site $2n$ (here we demonstrate for even sites), we perform the

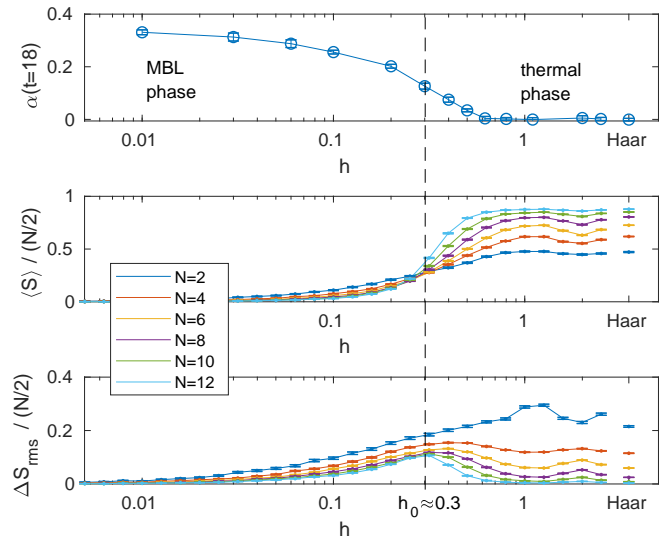


FIG. 5. MBL transition at $h_0 \approx 0.3$.

Top plot: Late-time value $\alpha(t = 18)$ (as in Fig. 4) as a function of the random coupling strength h , and (rightmost data-points) for Haar-distributed unitaries.

Middle and bottom plots: Average bipartite entanglement entropy (base 2) of eigenstates of 10^3 samples of the time evolution operator U , for several system sizes N . In addition to the average entropy of all eigenstates of a random instance U (middle) we calculate the standard deviation of the eigenstates of an instance (bottom). These measures show clear signals of an MBL transition that become more pronounced as the chain length N increases.

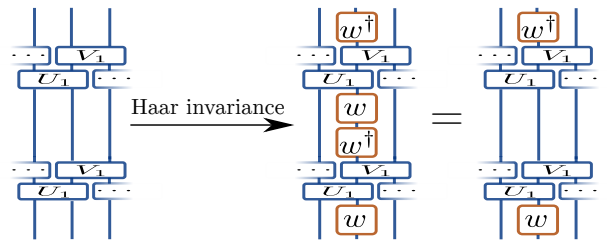


FIG. 6. Illustration of the twirling technique (see appendix IV A). By single-site Haar invariance, replacing $U_1 \rightarrow (\mathbb{I}_d \otimes w)U_1$ and $V_1 \rightarrow V_1(w^\dagger \otimes \mathbb{I}_d)$, $w \in U(d)$ does not affect the averaged result. The sketch shows an excerpt of the time evolution operator U . In a repeated application U^t , most w and w^\dagger cancel.

transformation

$$U_n \rightarrow (\mathbb{I}_d \otimes w_{2n})U_n; V_n \rightarrow V_n(w_{2n}^\dagger \otimes \mathbb{I}_d) \quad (18)$$

with arbitrary $w_{2n} \in U(d)$. Then w_{2n} cancels with w_{2n}^\dagger in a repeated application of the time evolution operator U , which transforms as

$$U^t \rightarrow w_{2n}^\dagger U^t w_{2n}, \quad (19)$$

w_{2n} only acting on site $2n$.

Thus Haar invariance allows us to relate the initial

state to the average final state:

$$\langle \rho_t \rangle = \langle U^t \rho_0 U^{t\dagger} \rangle = \langle w_{2n}^\dagger U^t w_{2n} \rho_0 w_{2n}^\dagger U^{t\dagger} w_{2n} \rangle \quad (20)$$

$$= w_{2n}^\dagger \langle \rho'_t \rangle w_{2n} \text{ with } \rho'_0 = w_{2n} \rho_0 w_{2n}^\dagger. \quad (21)$$

This holds for arbitrary $w_{2n} \in U(d)$ and can be iterated independently at each site. In some cases, it will prove useful to integrate over w_{2n} in (20), which, again, does not alter the result $\langle \cdot \rangle$. An important simplification arises when tracing over sites of the final state, because then in (20) the left- and rightmost w_{2n}^\dagger and w_{2n} cancel. In this paper we consider only distributions with single-site Haar invariance. Even in its absence, for example if transformation only with certain w_{2n} are allowed, some results may carry over.

B. Gaussian circuits: Inhomogeneous evolution

In this section, we show the result (11). First, we take $P_i, Q_i \in O(4)$. Then, we show how to reduce $P_i, Q_i \in SO(4)$ to the former case.

1. Haar measure on orthogonal group

By linearity of time evolution and Haar-averaging, it suffices to consider only initial states $\Gamma_0^n = \bigoplus_{i=1}^N \delta_{in} \gamma$ having all but site n maximally mixed. The 2×2 covariance matrix for the occupied site is given by $\gamma = \begin{pmatrix} 0 & 1 \\ -1 & 0 \end{pmatrix}$.

We adapt the twirling technique (section IV A) to the setting of Gaussian circuits to show that all components of $\langle \Gamma_t^n \rangle$ are zero, except the 2×2 block corresponding to on-site correlations at site n . To this end, consider the transformation

$$\bigoplus P_i \rightarrow \left(\bigoplus P_i \right) \Sigma; \quad \bigoplus Q_i \rightarrow G^\dagger \Sigma G \left(\bigoplus Q_i \right) \quad (22)$$

with a diagonal matrix Σ of signs ± 1 . Because Σ and $G^\dagger \Sigma G$ have the correct structure to be split among the P_i and Q_i , in spirit of the twirling technique we may perform this transformation using the Haar invariance of the Haar-distributed P_i, Q_i . Specifically, fix $\Sigma_{2n-1, 2n-1} = \Sigma_{2n, 2n} = +1$ such that $\Sigma \Gamma_0^n \Sigma = \Gamma_0^n$. Then, similarly to (20), single-site Haar invariance implies that

$$\langle \Gamma_t^n \rangle = \langle \Sigma O^t \Sigma \Gamma_0^n \Sigma O^{t\dagger} \Sigma \rangle = \Sigma \langle \Gamma_t^n \rangle \Sigma. \quad (23)$$

For each $i \neq 2n-1, 2n$, we are free to choose $\Sigma_{i,i} = -1$ and all other signs positive. From this we learn that the entire i 'th row and i 'th column (except the diagonal entry) of $\langle \Gamma_t^n \rangle$ are zero. The only matrix elements that can be non-zero are the diagonal and the 2×2 block corresponding to site n .

Moreover, the final covariance matrix is real antisymmetric, so the diagonal is also zero and only two entries $\langle \Gamma_t^n \rangle_{2n-1, 2n}, \langle \Gamma_t^n \rangle_{2n, 2n-1}$ remain. These form an antisymmetric 2×2 block at site n . Therefore this block is proportional to the same block of the initial covariance matrix;

we can write

$$\langle \Gamma_t^n \rangle = c(t, N, n) \Gamma_0^n. \quad (24)$$

It remains to show that $c(t, N, n)$ are equal for all n . The Haar average treats all unitaries on equal footing, such that within an average O possesses translational invariance by two sites. Therefore $\langle \Gamma_t^{n+2} \rangle = c(t, N, n) \langle \Gamma_0^{n+2} \rangle$, mandating that there can only be two distinct values for n even or odd.

Inversion of the chain corresponds to

$$P_i \rightarrow \left(\mathbb{I}_2 \right) P_{N/2-i} \left(\mathbb{I}_2 \right), \quad (25)$$

and accordingly for Q_i . It is a symmetry because in the average, $\left(\mathbb{I}_2 \right)$ can be Haar-absorbed by $P_{N/2-i}$. Inversion invariance implies that there is only one value $c(t, N) = c(t, N, n)$ for both n even and odd, the required form for (11). Any uncorrelated initial state can be decomposed as a linear combination of Γ_0^n 's, so by linearity, (11) holds with the same constant $c(t, N)$ for each initial state.

We state a few further conclusions. Note that the particle number of the state changes. Precisely we can formulate

$$c(t, N) = \frac{n(\langle \Gamma_t \rangle) / N - 1/2}{n(\Gamma_0) / N - 1/2} \quad (26)$$

because the particle number $n(\Gamma) = \sum (\lambda_i / 2 + 1/2)$ is related to the sum of every second entry λ_i along the state's first offdiagonal. Although we consider Gaussian circuits, transformations beyond those preserving particle number are of paramount importance in this setting (as $c(t, N) \neq 1$) and our results go beyond mere Anderson localization of a single particle.

After one time step, $c(t=1, N) = 0$ exactly, as direct integration of P_i, Q_i shows [39]. After that, it becomes non-zero. To assess the localising properties of the system, the long-time behaviour of $c(t, N)$ is of interest. For this, its time average

$$c(t\text{-avg}, N) := \lim_{T \rightarrow \infty} \frac{1}{T} \sum_{t=0}^{T-1} c(t, N) \quad (27)$$

is a useful value. This removes the dependence on the eigenvalues $e^{i\theta_i}$ of O : From (11) we can write

$$c(t, N) = -\frac{1}{2} \langle \text{Tr} \Gamma_0^n O^t \Gamma_0^n O^{t\dagger} \rangle \quad (28)$$

for any $1 \leq n \leq N$. Inserting the spectral decomposition $O = \sum_i |v_i\rangle e^{i\theta_i} \langle v_i|$, the generic non-degenerate case $\theta_i \neq$

θ_j yields

$$c(t\text{-avg}, N) = -\frac{1}{2} \left\langle \sum_{i,j} \overbrace{\lim_{T \rightarrow \infty} \frac{1}{T} \sum_{t=0}^{T-1} e^{i\theta_i t - i\theta_j t}}^{\delta_{ij}} \right\rangle \quad (29)$$

$$\begin{aligned} & \left\langle \text{Tr} \Gamma_0^n |v_i\rangle \langle v_i| \Gamma_0^n |v_j\rangle \langle v_j| \right\rangle \\ &= \frac{1}{2} \left\langle \sum_{i=1}^{2N} |\langle v_i | \Gamma_0^n | v_i \rangle|^2 \right\rangle \geq 0 \end{aligned} \quad (30)$$

While it is expected that this average is strictly positive, its scaling in the thermodynamic limit $N \rightarrow \infty$ is unclear. To establish that $c(t, N)$ reaches a finite value and localization holds, we resort to numerical calculations of $c(t, N)$ as shown in Fig. 2.

2. Haar measure on special orthogonal group

We will now show that the results for the $O(4)$ Haar measure equally apply when using the $SO(4)$ Haar measure. Let the number of timesteps $t < (N-1)/2$, such that the lightcone fits into the periodic system without overlapping. Relate the orthogonal to the special orthogonal group by writing $P_i, Q_i \in O(4)$ in the form

$$P_i = \begin{pmatrix} 1 & & & \\ & 1 & & \\ & & 1 & \\ & & & -1 \end{pmatrix}^{p_i} \tilde{P}_i, \quad Q_i = \tilde{Q}_i \begin{pmatrix} 1 & & & \\ & -1 & & \\ & & 1 & \\ & & & -1 \end{pmatrix}^{q_i} \quad (31)$$

with $\tilde{P}_i, \tilde{Q}_i \in SO(4)$ and $p_i, q_i \in \mathbb{Z}_2$. Note that the orthogonal Haar distribution for P_i corresponds to the special orthogonal Haar distribution for \tilde{P}_i in combination with the uniform distribution for p_i .

Our strategy will consist in showing that the average

$$\langle O^t \Gamma_0^n O^{t\dagger} \rangle_{P_i, Q_i \in O(4)} = \left\langle \langle O^t \Gamma_0^n O^{t\dagger} \rangle_{\tilde{P}_i, \tilde{Q}_i \in SO(4)} \right\rangle_{p_i, q_i \in \mathbb{Z}_2} \quad (32)$$

$$= \langle O^t \Gamma_0^n O^{t\dagger} \rangle_{\substack{\tilde{P}_i, \tilde{Q}_i \in SO(4) \\ p_i, q_i \text{ fixed}}} = \langle O^t \Gamma_0^n O^{t\dagger} \rangle_{P_i, Q_i \in SO(4)} \quad (33)$$

is independent of how p_i, q_i are fixed, i.e. the equality of (32) and (33). Then the equality of $O(4)$ and $SO(4)$ averages immediately follows for all states; these can be written as linear combinations of Γ_0^n 's. We may absorb all q_i into p_i by the transformation $q_i \rightarrow 0, p_i \rightarrow p_i + q_i$ which uses associativity of matrix multiplication to regroup q_i from \tilde{Q}_i to p_i and \tilde{P}_i .

Thanks to $SO(4)$ Haar invariance of \tilde{Q}_k and \tilde{P}_{k+1} (for each index k in turn), whenever $p_k = 1$ we may perform the transformation $p_k \rightarrow 0, p_{k+1} \rightarrow p_{k+1} + 1$. Specifically, this follows from the $SO(4)$ -Haar-invariant transformations

$$\tilde{Q}_k \rightarrow \tilde{Q}_k \begin{pmatrix} 1 & & & \\ & -1 & & \\ & & 1 & \\ & & & -1 \end{pmatrix}, \quad \tilde{P}_{k+1} \rightarrow \begin{pmatrix} 1 & & & \\ & -1 & & \\ & & 1 & \\ & & & -1 \end{pmatrix} \tilde{P}_{k+1}. \quad (34)$$

Iterating this transformation for increasing values of k , we may set all $p_i = 0$ except for $p_{N/2}$ which may be 0 or 1. Due to the lightcone size, all occurrences of $p_{N/2}$ are multiplied by the zeros in the initial state $\Gamma_0^n = \bigoplus_i \delta_{in} \gamma$ (for $n = N/2$, other initial sites n follow similarly). In conclusion, the average (33) is independent of all p_i, q_i and the main result (11) holds for both the $O(4)$ and $SO(4)$ Haar measures.

C. Gaussian circuits: Homogeneous evolution

In this section, the time evolution operator O is homogeneous, $P = P_i = P_j \in O(4), Q = Q_i = Q_j \in O(4)$. We show the result (12) summarized in section III A 2.

a. Fourier transformation of problem. First, let us perform a Fourier transformation of the problem. The periodic structure of O suggests a Fourier transform of two-site blocks with $\mathcal{F} \otimes \mathbb{I}_4$, employing the $N/2 \times N/2$ discrete Fourier matrix

$$\mathcal{F}_{kj} := \frac{1}{\sqrt{N/2}} \exp\left(-2\pi i \frac{(k-1)(j-1)}{N/2}\right), \quad (35)$$

where $k, j = 1 \dots N/2$. We will denote Fourier transformed quantities with a hat. The time evolution operator O is block-circulant (4), hence its Fourier transform is block-diagonal and can be written in terms of the diagonal components

$$O \xrightarrow{\mathcal{F} \otimes \mathbb{I}_4} \bigoplus_{k=1}^{N/2} \hat{O}_k, \quad \hat{O}_k = \hat{G}_k Q \hat{G}_k^\dagger P \in U(4), \quad (36)$$

with $\hat{G}_k := \begin{pmatrix} 0 & \exp(2\pi i k / (N/2)) \mathbb{I}_2 \\ \mathbb{I}_2 & 0 \end{pmatrix}$.

b. Localized initial state. Consider now the localized initial state $\Gamma_0^n = \bigoplus_{i=1}^N \delta_{in} \gamma$ with site n occupied (wlog we consider n odd) and all other sites maximally mixed. Its Fourier transform is not block-diagonal as for the time evolution operator (36), but also has off-diagonal blocks

$$\Gamma_0^n \xrightarrow{\mathcal{F} \otimes \mathbb{I}_4} (\hat{\Gamma}_0^n)_{kl} = \frac{1}{N/2} e^{i\phi_{kl}} (\gamma_0) \quad (37)$$

with phases $\phi_{kl} = 2\pi(n-1)(k-l)/N$. Accordingly, the final state has off-diagonal blocks, too:

$$\langle \Gamma_t^n \rangle \xrightarrow{\mathcal{F} \otimes \mathbb{I}_4} \langle \hat{\Gamma}_t^n \rangle_{kl} = \frac{1}{N/2} e^{i\phi_{kl}} \langle \hat{O}_k^t (\gamma_0) \hat{O}_l^{t\dagger} \rangle. \quad (38)$$

Numerical calculations provide evidence that all blocks $\langle \hat{\Gamma}_t^n \rangle_{kl}$ vanish as $t \rightarrow \infty$, except for the diagonal $k = l$, and the pairs $(k, l) = (N/2, N/4), (k, l) = (N/4, N/2)$. These pairs only exist for N divisible by four and correspond to the Fourier phases 0 and π . Only for these two pairs are both \hat{O}_k and \hat{O}_l real.

c. Time-average for localized initial state. As we now argue, in the time average $\langle \Gamma_{t\text{-avg}}^n \rangle$ all Fourier blocks $\langle \hat{\Gamma}_{t\text{-avg}}^n \rangle_{kl}, k \neq l, (k, l) \neq (N/2, N/4), (k, l) \neq (N/4, N/2)$

are zero. Inserting the spectral decomposition $\hat{O}_k = \sum_{i=1}^4 e^{i\theta_{k,i}} |v_{k,i}\rangle\langle v_{k,i}|$, the time average is

$$\langle \hat{\Gamma}_{t\text{-avg}}^n \rangle_{kl} = \frac{e^{i\phi_{kl}}}{N/2} \left\langle \sum_{i,j=1}^4 \overbrace{\lim_{T \rightarrow \infty} \frac{1}{T} \sum_{t=0}^{T-1} e^{i(\theta_{k,i} - \theta_{l,j})t}}^{(*)} |v_{k,i}\rangle\langle v_{k,i}| (\gamma_0) |v_{l,j}\rangle\langle v_{l,j}| \right\rangle. \quad (39)$$

For each fixed pair (k, l) , whenever the sets of eigenvalues $\{e^{i\theta_{k,i}}, i = 1, 2, 3, 4\}$ of \hat{O}_k and $\{e^{i\theta_{l,i}}, i = 1, 2, 3, 4\}$ of \hat{O}_l are disjoint, $(*)$ is zero. Moreover, for the Haar average $\langle \hat{\Gamma}_{t\text{-avg}}^n \rangle_{kl}$ to vanish for any given pair (k, l) , it suffices that the eigenvalue sets are disjoint for all P, Q except a measure zero set. We conjecture that this holds for all pairs $(k, l), k \neq l$ and $(k, l) \neq (N/2, N/4), (k, l) \neq (N/4, N/2)$ [40].

In conclusion, in the time average of (38) of an initially localized state, only Fourier components $k = l$ and $k, l = N/2, N/4$ survive:

$$\langle \Gamma_{t\text{-avg}}^n \rangle \xrightarrow{\mathcal{F} \otimes \mathbb{I}_4} \langle \hat{\Gamma}_{t\text{-avg}}^n \rangle_{kl} = \quad (40a)$$

$$\frac{\delta_{k=l}}{N/2} \lim_{T \rightarrow \infty} \frac{1}{T} \sum_{t=0}^{T-1} \langle \hat{O}_k^t (\gamma_0) \hat{O}_k^{t\dagger} \rangle \quad (40b)$$

$$+ \frac{\delta_{k=N/2, l=N/4} + \delta_{k=N/4, l=N/2}}{N/2} \quad (40c)$$

$$e^{i\phi_{kl}} \lim_{T \rightarrow \infty} \frac{1}{T} \sum_{t=0}^{T-1} \langle \hat{O}_k^t (\gamma_0) \hat{O}_l^{t\dagger} \rangle. \quad (40d)$$

Note that the position n of the initial localization is present in (40b) only as $n \bmod 2$, determining (γ_0) or (γ) , and in (40d) only as $n \bmod 4$, in the phase $\phi_{kl} = 2\pi(n-1)(k-l)/N = \pm\pi/2(n-1)$.

The Fourier backtransformation is

$$\langle \Gamma_{t\text{-avg}}^n \rangle = \frac{1}{N/2} \Gamma_{\star} := \frac{1}{N/2} (\Gamma'_{\star} + \Gamma''_{\star}), \quad (41)$$

where Γ'_{\star} denotes the backtransform arising from the diagonal Fourier components (40b) and Γ''_{\star} the backtransform arising from the Fourier components $k, l = N/2, N/4$ (40d), each without the prefactor $1/(N/2)$. As discussed in the previous paragraph, Γ_{\star} is only dependent on $n \bmod 4$ and, thanks to the prefactor, vanishes in the limit $N \rightarrow \infty$. This concludes our result (12).

d. Translation-invariant initial state. On top of the results summarized in section III A 2, we provide a characterization of Γ'_{\star} . For this, we need to first consider the translation-invariant initial state $\Gamma_0^{\text{t.i.}}$ with each site occupied. It is invariant under Fourier transformation:

$$\Gamma_0^{\text{t.i.}} = \bigoplus_{i=1}^N \gamma \xrightarrow{\mathcal{F} \otimes \mathbb{I}_4} \hat{\Gamma}_0^{\text{t.i.}} = \bigoplus_{k=1}^{N/2} (\gamma_{\gamma}). \quad (42)$$

The final state has a block-diagonal Fourier transform and each block has the form

$$\langle \Gamma_t^{\text{t.i.}} \rangle = \langle O^t \Gamma_0^{\text{t.i.}} O^{t\dagger} \rangle \xrightarrow{\mathcal{F} \otimes \mathbb{I}_4} \langle \hat{\Gamma}_t^{\text{t.i.}} \rangle_k = \langle \hat{O}_k^t (\gamma_{\gamma}) \hat{O}_k^{t\dagger} \rangle. \quad (43)$$

We will now relate the translation-invariant state's time average $\langle \Gamma_{t\text{-avg}}^{\text{t.i.}} \rangle$ to Γ'_{\star} in the time average of localized initial states.

e. Relating Γ'_{\star} to $\langle \Gamma_{t\text{-avg}}^{\text{t.i.}} \rangle$. We now show that $\Gamma'_{\star} = \langle \Gamma_{t\text{-avg}}^{\text{t.i.}} \rangle$ except that all rows and columns corresponding to even sites are zero. For this, we exploit Haar invariance, similarly to the twirling technique and the case of inhomogeneous fermionic time evolution. The twirling technique can be used either with the original time evolution operator (4) and (6) or equivalently directly in the Fourier transformed quantities (36) and (43), which in the following is the perspective we take.

First, we show that $\langle \hat{\Gamma}_t^{\text{t.i.}} \rangle_k$ (see (43)) is 2×2 block-diagonal. This follows from the transformation

$$P \rightarrow P\Sigma, Q \rightarrow \hat{G}_k^{\dagger} \Sigma^{\dagger} \hat{G}_k Q \quad (44)$$

with $\Sigma = \begin{pmatrix} \pm\mathbb{I}_2 & \\ & \pm\mathbb{I}_2 \end{pmatrix}$. Note that $\hat{G}_k^{\dagger} \Sigma^{\dagger} \hat{G}_k$ is real orthogonal as required to apply $O(4)$ Haar invariance. This transformation effects, as in (20),

$$\langle \hat{\Gamma}_t^{\text{t.i.}} \rangle_k = \langle \Sigma^{\dagger} \hat{O}_k^t \Sigma (\gamma_{\gamma}) \Sigma^{\dagger} \hat{O}_k^{t\dagger} \Sigma \rangle = \Sigma^{\dagger} \langle \hat{\Gamma}_t^{\text{t.i.}} \rangle_k \Sigma. \quad (45)$$

With appropriate choice of signs in Σ it follows that the off-diagonal blocks of $\langle \hat{\Gamma}_t^{\text{t.i.}} \rangle_k$ vanish.

Now we are in a position to show the relation between $\langle \hat{O}_k^t (\gamma_{\gamma}) \hat{O}_k^{t\dagger} \rangle$ and $\langle \hat{O}_k^t (\gamma_0) \hat{O}_k^{t\dagger} \rangle$ appearing in the Fourier transformations of $\langle \Gamma_{t\text{-avg}}^{\text{t.i.}} \rangle$ and Γ'_{\star} , respectively. For this, use the transformation (44) with

$$\Sigma = \begin{pmatrix} 1 & \\ & 1 \ 0 \end{pmatrix}. \quad (46)$$

Again, note $\hat{G}_k^{\dagger} \Sigma \hat{G}_k$ is real. Then

$$\langle \hat{O}_k^t (\gamma_0) \hat{O}_k^{t\dagger} \rangle = \frac{1}{2} \left[\langle \hat{O}_k^t (\gamma_{\gamma}) \hat{O}_k^{t\dagger} \rangle + \langle \hat{O}_k^t (\gamma_{-\gamma}) \hat{O}_k^{t\dagger} \rangle \right] \quad (47)$$

$$= \frac{1}{2} \left[\langle \hat{O}_k^t (\gamma_{\gamma}) \hat{O}_k^{t\dagger} \rangle + \langle \hat{O}_k^t \Sigma (\gamma_{\gamma}) \Sigma \hat{O}_k^{t\dagger} \rangle \right]$$

$$= \frac{1}{2} \left[\langle \hat{O}_k^t (\gamma_{\gamma}) \hat{O}_k^{t\dagger} \rangle + \Sigma \langle \hat{O}_k^t (\gamma_{\gamma}) \hat{O}_k^{t\dagger} \rangle \Sigma \right],$$

with the last equality due to Haar invariance. Thanks to one term without and one term conjugated by Σ , the first block stays the same and the second block (which corresponds to even sites) cancels. This carries through the Fourier transform $\mathcal{F} \otimes \mathbb{I}_4$, concluding our proof that $\Gamma'_{\star} = \langle \Gamma_{t\text{-avg}}^{\text{t.i.}} \rangle$ except that all rows and columns corresponding to even sites are zero.

f. Characterization of $\langle \Gamma_t^{\text{t.i.}} \rangle$. Now we will further characterize $\langle \Gamma_t^{\text{t.i.}} \rangle$ arising from the translation-invariant initial state. In terms of the Fourier components of $\langle \Gamma_t^{\text{t.i.}} \rangle$, we show below that

$$\langle \hat{\Gamma}_t^{\text{t.i.}} \rangle_k = c(t, k, N) (\gamma_{\gamma}), \quad (48)$$

with a real constant $c(t, k, N)$. This is a similar form as the main result (11) except that there is one constant per Fourier component. The methods in the proof following are also very similar.

We have shown already that $\langle \hat{\Gamma}_t^{t.i.} \rangle_k$ consists of two 2×2 blocks, in the paragraph of equation (44). $\langle \hat{\Gamma}_t^{t.i.} \rangle_k$ is evidently anti-hermitian as a real antisymmetric matrix conjugated with a unitary (43). To prove (48), it remains to show that both blocks are real and identical.

First, we show that both blocks are real. To this end, use the transformation (44) with

$$\Sigma = \begin{pmatrix} 0 & 1 \\ -1 & 0 \\ & 0 & 1 \\ & -1 & 0 \end{pmatrix}. \quad (49)$$

Note that $\hat{G}_k^\dagger \Sigma^\dagger \hat{G}_k$ is real orthogonal, so Haar invariance of P and Q 's probability distribution is applicable. For anti-hermitian 2×2 matrices X ,

$$X = \begin{pmatrix} 0 & 1 \\ -1 & 0 \end{pmatrix}^\dagger X \begin{pmatrix} 0 & 1 \\ -1 & 0 \end{pmatrix} \Rightarrow X \text{ real antisymmetric.} \quad (50)$$

Therefore, the transformation's effect (45) shows that both blocks are real.

Lastly, we show that both blocks are identical. This is achieved by considering inversion symmetry of the chain. Inversion corresponds to

$$P \rightarrow \begin{pmatrix} & \mathbb{I}_2 \\ \mathbb{I}_2 & \end{pmatrix} P \begin{pmatrix} & \mathbb{I}_2 \\ \mathbb{I}_2 & \end{pmatrix} \quad (51)$$

and likewise for Q . This is equivalent to

$$\hat{O}_k \rightarrow \begin{pmatrix} & \mathbb{I}_2 \\ \mathbb{I}_2 & \end{pmatrix} \hat{O}_k^* \begin{pmatrix} & \mathbb{I}_2 \\ \mathbb{I}_2 & \end{pmatrix} \quad (52)$$

and

$$\langle \hat{\Gamma}_t^{t.i.} \rangle_k \rightarrow \begin{pmatrix} & \mathbb{I}_2 \\ \mathbb{I}_2 & \end{pmatrix} \langle \hat{\Gamma}_t^{t.i.} \rangle_k^* \begin{pmatrix} & \mathbb{I}_2 \\ \mathbb{I}_2 & \end{pmatrix}. \quad (53)$$

Thus inversion invariance mandates that both real blocks are the same.

g. Characterization of $c(t, k, N)$. To understand $\langle \Gamma_t^{t.i.} \rangle$, it remains to characterize $c(t, k, N)$. In Fig. 7 we therefore show numerical calculations of $c(t, k, N)$.

The figure shows that $c(t, k, N)$ converges, except for $\frac{2\pi}{N/2}k = 0, \pi, 2\pi$, where there are oscillations in t . We can calculate the time average of values

$$c(t\text{-avg}, k, N) = \frac{1}{4} \text{ for } \frac{2\pi}{N/2}k = 0, \pi, 2\pi \quad (54)$$

exactly. In these cases, \hat{G}_k is real orthogonal and can be absorbed by the Haar-invariant transformation $Q \rightarrow \hat{G}_k^\dagger Q \hat{G}_k$. In turn, Q can be absorbed by the transformation $P \rightarrow Q^\dagger P$. Then we have simply $\hat{O}_k = P$; this corresponds to two sites in the uncoupled case and is explained in appendix A.

The symmetries $k \leftrightarrow -k = N/2 - k$ and " $k \leftrightarrow k + \pi$ " of $c(t, k, N)$ are apparent in Fig. 7. The first corresponds to complex conjugation of \hat{O}_k , and is a symmetry because $\langle \Gamma_t^{t.i.} \rangle_k$ is real. The latter symmetry only exists for even

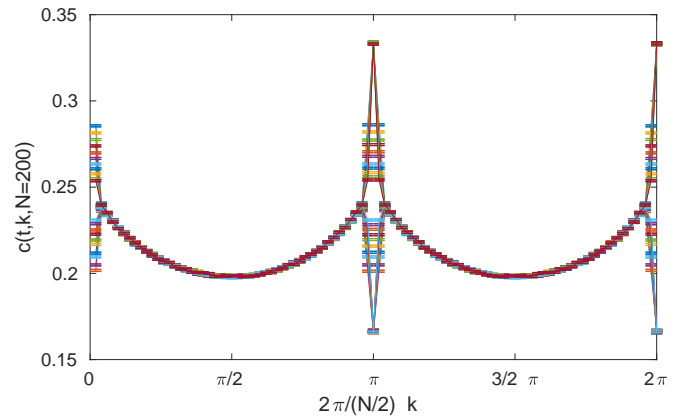


FIG. 7. Constant $c(t, k, N = 200)$ for the characterization of $\langle \Gamma_t^{t.i.} \rangle$ (48) for homogeneous evolution of fermions. Each of the lines shows data for a fixed t from 20 to 50. We perform the orthogonal Haar average by considering 10^6 samples.

$N/2$ and then reads $k \leftrightarrow k + N/4$. It is equivalent to the Haar-invariant transformation

$$Q \rightarrow \begin{pmatrix} -\mathbb{I}_2 & \\ & \mathbb{I}_2 \end{pmatrix} Q \begin{pmatrix} \mathbb{I}_2 & \\ & -\mathbb{I}_2 \end{pmatrix} \quad (55)$$

which effects $e^{\pm 2\pi i k / (N/2)} \rightarrow -e^{\pm 2\pi i k / (N/2)}$ in (36).

1. Homogeneous evolution — Eigenvector delocalization

In this section, we explain in detail a complementary viewpoint to delocalization summarized in section III A 2, eigenvector delocalization. The eigenvectors \vec{v}_i to eigenvalues $e^{i\theta_i}$ of each generic instance of the homogeneous evolution operator O are delocalized. To see this, let \mathcal{T} be the orthogonal operator effecting translation by two sites (4 matrix entries). It commutes with O and has $\mathcal{T}^{N/2} = \mathbb{I}_{2N}$. Each \vec{v}_i is therefore eigenvector of \mathcal{T} to a phase ϕ_i and for its components the relation $v_i^{j+4} = e^{i\phi_i} v_i^j$ holds circularly. Taking \vec{v}_i normalized,

$$|v_i^j|^2 = \frac{2}{N} \left(\sum_{k=0}^{N/2-1} |v_i^{j+4k}|^2 \right) \leq \frac{2}{N} |v_i|^2 = \frac{2}{N}. \quad (56)$$

In the generic case, where O does not have degenerate eigenvalues, we can give an estimate of the final covariance matrix even without resorting to a Haar average. We expand $\Gamma_{t\text{-avg}}^n$ with the spectral decomposition $O = \sum_k |v_k\rangle e^{i\theta_k} \langle v_k|$ of the specific instance of the time evolution operator:

$$\Gamma_{t\text{-avg}}^n = \lim_{T \rightarrow \infty} \frac{1}{T} \sum_{t=0}^{T-1} O^t \Gamma_0^n O^{t\dagger} \quad (57)$$

$$= \sum_{k,l=1}^{2N} \overbrace{\lim_{T \rightarrow \infty} \frac{1}{T} \sum_{t=0}^{T-1} e^{i(\theta_k - \theta_l)t}}^{\delta_{\theta_k, \theta_l}} |v_k\rangle \langle v_k| \Gamma_0^n |v_l\rangle \langle v_l|. \quad (58)$$

Similarly to (29), the time average cancels cross terms.

Let \vec{e}_j be the standard basis. The matrix elements of $\Gamma_{t\text{-avg}}^n$ are then

$$\langle e_i | \Gamma_{t\text{-avg}}^n | e_j \rangle = \sum_{k=1}^{2N} \langle e_i | v_k \rangle \langle v_k | \Gamma_0^n | v_k \rangle \langle v_k | e_j \rangle. \quad (59)$$

With the bound (56) for the eigenvector's components, we can show the estimate (13) by expanding $\Gamma_0^n = |e_{2n-1}\rangle\langle e_{2n}| - |e_{2n}\rangle\langle e_{2n-1}|$:

$$|(\Gamma_{t\text{-avg}}^n)_{ij}| = |\langle e_i | \Gamma_{t\text{-avg}}^n | e_j \rangle| \quad (60)$$

$$\leq \sum_{k=1}^{2N} \underbrace{|\langle e_i | v_k \rangle|}_{\leq \sqrt{2/N}} \underbrace{|\langle v_k | \Gamma_0^n | v_k \rangle|}_{\leq 4/N} \underbrace{|\langle v_k | e_j \rangle|}_{\leq \sqrt{2/N}} \leq \frac{16}{N} \quad (61)$$

D. Spins

In this section we prove our analytic results about spin chains summarized in section III B 1, using the twirling technique from section IV A. We require the probability distribution for the unitaries U_i, V_i comprising the unitary-circuit time evolution operator to possess single-site Haar invariance, as introduced in the settings II B.

The integral over the unitary group

$$\begin{aligned} & \int_{U(d)} dw_n w_n^\dagger A w_n B_n w_n^\dagger C w_n \quad (62) \\ &= \frac{\mathbb{I}_d^n}{d} \text{Tr}_n(B_n) \otimes \frac{d \text{Tr}_n(AC) - \text{Tr}_n(A) \text{Tr}_n(C)}{d^2 - 1} \\ &+ B_n \otimes \frac{d \text{Tr}_n(A) \text{Tr}_n(C) - \text{Tr}_n(AC)}{d(d^2 - 1)} \end{aligned}$$

can be computed exactly [41]. Here $A, C \in U(d^N)$ are multi-qudit operators and $w_n, B_n \in U(d)$ act only on one qudit at site n . The left side of the tensor products is qudit n while the right side contains all the other sites. The same result is obtained when averaging over a unitary 2-design such as, for qubits, the Clifford group [42] instead of entire $U(d)$.

Similarly, we have the integral

$$\int_{U(d)} dw_i w_i D w_i^\dagger = \text{Tr}_i(D) \otimes \mathbb{I}_d^i/d, \quad (63)$$

where $D \in U(d^N)$ is a multi-qudit operator and $w_i \in U(d)$ acts only on one qudit at site i . The identity \mathbb{I}_d^i/d is at the qudit site i which is traced out from D . The integral holds equally for the integrand $w_i^\dagger D w_i$. For this integral, a unitary 1-design is sufficient for w_i , such as for $d = 2$ the Pauli matrices together with the identity.

To show our result (15) for a single-site reduced density matrix at site n , let $I = \{1 \dots N\} \setminus \{n\}$ be the set of all other sites. Let ρ_0 be the (arbitrary) initial state.

With this notation, we will compute the relation between $\text{Tr}_I \rho_0$ and

$$\text{Tr}_I \langle \rho_t \rangle = \text{Tr}_I \langle U^t \rho_0 U^{t\dagger} \rangle. \quad (64)$$

At each site $i \in I$ in turn, the twirling technique (20) results in

$$\text{Tr}_I \langle \rho_t \rangle = \text{Tr}_I \langle w_i^\dagger U^t w_i \rho_0 w_i^\dagger U^{t\dagger} w_i \rangle = \text{Tr}_I \langle U^t w_i \rho_0 w_i^\dagger U^{t\dagger} \rangle. \quad (65)$$

We may integrate over w_i , whose choice is arbitrary, by setting $D = \rho_0$ in formula (63). This gives

$$\text{Tr}_I \langle \rho_t \rangle = \text{Tr}_I \langle U^t [\text{Tr}_i(\rho_0) \otimes \mathbb{I}_d^i/d] U^{t\dagger} \rangle. \quad (66)$$

Iteration of this procedure for each $i \in I$ yields

$$\text{Tr}_I \langle \rho_t \rangle = \text{Tr}_I \langle U^t [\text{Tr}_I(\rho_0) \otimes \mathbb{I}_{d^{N-1}}^I/d^{N-1}] U^{t\dagger} \rangle. \quad (67)$$

The twirling technique at site n allows us to use formula (62) with $A = U^t, B_n = \text{Tr}_I(\rho_0), C = U^{t\dagger}$:

$$\text{Tr}_I \langle \rho_t \rangle = \frac{1}{d^{N-1}} \text{Tr}_I \langle w_n^\dagger U^t w_n \text{Tr}_I(\rho_0) w_n^\dagger U^{t\dagger} w_n \rangle \quad (68)$$

$$= \frac{1}{d^{N-1}} \text{Tr}_I \left\langle \frac{\mathbb{I}_d^n}{d} \text{Tr}_n \text{Tr}_I(\rho_0) \otimes \quad (69)$$

$$\frac{d \text{Tr}_n(AC) - \text{Tr}_n A \text{Tr}_n C}{d^2 - 1} \quad (70)$$

$$+ \text{Tr}_I(\rho_0) \otimes \frac{d \text{Tr}_n A \text{Tr}_n C - \text{Tr}_n(AC)}{d(d^2 - 1)} \right\rangle \quad (71)$$

$$= \frac{\mathbb{I}_d^n}{d} \frac{d^2 - \lambda(t)}{d^2 - 1} + \text{Tr}_I(\rho_0) \frac{\lambda(t) - 1}{d^2 - 1} \quad (72)$$

$$= \frac{\mathbb{I}_d^n}{d} + \underbrace{\frac{\lambda(t) - 1}{d^2 - 1}}_{\alpha(t)} \bar{\rho}_0^n. \quad (73)$$

In the third equality we have used that $\text{Tr}_n \text{Tr}_I(\rho_0) = 1$, $\text{Tr}_I \text{Tr}_n(AC) = d^N$ and defined the constant

$$\lambda(t) = \left\langle \frac{1}{d^{N-1}} \text{Tr}_I(\text{Tr}_n U^t \text{Tr}_n U^{t\dagger}) \right\rangle \quad (74)$$

into which we have moved the remaining Haar average. λ is manifestly real and non-negative. In the final equality we have rewritten the expression in terms of the traceless part $\bar{\rho}_0^n$ of the initial reduced density matrix $\text{Tr}_I \rho_0$. The form (15) of our result can be obtained by setting $\alpha(t) = \frac{\lambda(t) - 1}{d^2 - 1}$.

A lightcone structure emerges in the definition of λ . Only constituent unitaries of U within a lightcone of velocity 2 around site n contribute to λ , all others cancel with their daggered counterpart in consequence of Tr_I . A longer chain will have an additional $\text{Tr}_i(\mathbb{I}_d)$ at each additional site i outside the lightcone, which is precisely cancelled by the higher N in the prefactor. (Fig. 8 shows a graphical representation of a slightly different quantity but also serves to illustrate this fact.) In combination with Haar invariance of U , within the average $\langle \cdot \rangle$ that

treats all constituent unitaries on equal footing, we realize the following. $\lambda(t)$ is independent of site position n or chain length N as long as the lightcone around n does not intersect a boundary, or, in the case of periodic boundary conditions, itself.

After a single timestep, $\lambda(1) = 1$ exactly such that the evolution results in a locally maximally mixed site (73). For longer times, we resort to a numerical method for evaluating $\alpha(t) = \frac{\lambda(t)-1}{d^2-1}$, explained in the next section V.

Next let us calculate the entire final density matrix $\langle \rho_t \rangle$ for the initial state

$$\rho_0 = \rho_0^n \otimes \mathbb{I}_{d^{N-1}}^I / d^{N-1} \quad (75)$$

that has all sites maximally mixed apart from site n . The twirling technique and formula (63) with $D = U^t \rho_0 U^{t\dagger}$ can be applied at each site $i \in I$ iteratively:

$$\langle \rho_t \rangle = \langle w_i^\dagger U^t w_i \rho_0 w_i^\dagger U^{t\dagger} w_i \rangle = \langle w_i^\dagger U^t \rho_0 U^{t\dagger} w_i \rangle \quad (76)$$

$$= \langle \text{Tr}_i(U^t \rho_0 U^{t\dagger}) \rangle \otimes \mathbb{I}_d^i / d \quad (77)$$

$$= \langle \text{Tr}_I(U^t \rho_0 U^{t\dagger}) \rangle \otimes \mathbb{I}_{d^{N-1}}^I / d^{N-1} \quad (78)$$

$$= \text{Tr}_I \langle \rho_t \rangle \otimes \mathbb{I}_{d^{N-1}}^I / d^{N-1}. \quad (79)$$

All sites of the final state are maximally mixed except for site n , it is related to the initial $\rho_0^n = \text{Tr}_I(\rho_0)$ as per (72).

Let us turn to the behaviour of two-site reduced density matrices for the not necessarily adjacent sites n and m , now $I = \{1 \dots N\} \setminus \{n, m\}$. Assume the initial state's reduced density matrix to be a tensor product and split it

$$\text{Tr}_I(\rho_0) = (\mathbb{I}_d^n / d + \bar{\rho}_0^n) \otimes (\mathbb{I}_d^m / d + \bar{\rho}_0^m) \quad (80)$$

into traceful and traceless parts.

To determine the final state $\text{Tr}_I \langle \rho_t \rangle$, we employ the same method as before. However we will have to use formula (62) twice, at sites n and m , and the resulting Tr_n and Tr_m terms couple. A calculation yields the compact result

$$\begin{aligned} \text{Tr}_I \langle \rho_t \rangle &= \left(\frac{\mathbb{I}_d^n}{d} + \frac{\lambda - 1}{d^2 - 1} \bar{\rho}_0^n \right) \otimes \left(\frac{\mathbb{I}_d^m}{d} + \frac{\lambda - 1}{d^2 - 1} \bar{\rho}_0^m \right) \\ &+ \frac{\lambda' - \lambda^2}{(d^2 - 1)^2} \bar{\rho}_0^n \otimes \bar{\rho}_0^m. \end{aligned} \quad (81)$$

Here $\lambda = \lambda(t)$ is the same as before in (74), so the first term is simply an uncorrelated tensor product of the single site result (73). The coefficient

$$\lambda'(t) = \left\langle \frac{1}{d^{N-2}} \text{Tr}_I(\text{Tr}_{n,m} U^t \text{Tr}_{n,m} U^{t\dagger}) \right\rangle \quad (82)$$

appearing in the second term is also real and positive. It depends on $|n - m|$ until the sites are far enough apart such that their lightcones do not intersect. (This requires a sufficient system size.) In that case, $\lambda' = \lambda^2$ and the two-site result (81) reduces to the single site result (73).

Our method to show that the evolution of a single site is a depolarising channel (73) may readily be generalized to further time evolutions other than the specific quantum circuit considered here. For this, the time evolution operator must allow for transformations of the form (19), such that the twirling technique can be applied analogously. One such example was studied in [43, 44], which considered a random non-local Hamiltonian coupling all N spins, whose diagonalising matrix is distributed according to the $U(d^N)$ Haar measure. In that case, the expression for $\alpha(t)$ can be simplified in terms of the spectral form factor of the Hamiltonian.

V. NUMERICAL METHOD FOR SPINS

In this section, we present the new numerical method we use for the setting of spin chains. Obtaining numerical values for $\alpha(t)$ of (15) is much more difficult than for $c(t, N)$ in the fermionic case, because the Hilbert space grows exponentially while covariance matrices grow only quadratically in system size N . In the following, we describe a new numerical method that significantly decreases the complexity from 4^{2t+1} to 2^t for t timesteps, at effectively infinite system size. For definiteness, we set the local Hilbert space dimension $d = 2$ although our numerical method can be adapted to higher spins.

We determine $\alpha(t)$ by preparing an initial state where one site is spin up $|0\rangle\langle 0|$ and all other sites are maximally mixed. After applying U^t , we project the final reduced density matrix of the one site onto $|0\rangle\langle 0|$. According to (15), this procedure yields

$$(\alpha + 1)/2 = \langle R(U, 0) \rangle_U, \quad (83)$$

$$\begin{aligned} R(U, s) &= \text{Tr} \left[(\dots \otimes \mathbb{I}_2 \otimes (|s\rangle\langle s|) \otimes \mathbb{I}_2 \otimes \dots) \right. \\ &\left. U^t (\dots \otimes \mathbb{I}_2 / 2 \otimes (|0\rangle\langle 0|) \otimes \mathbb{I}_2 / 2 \otimes \dots) U^{t\dagger} \right]. \end{aligned} \quad (84)$$

The average $\langle \cdot \rangle_U$ refers to averaging the random U_i, V_i composing U . Leaving the final spin s free allows us to use an importance sampling technique. Before explaining this technique, we will show how to evaluate $R(U, s)$ for a given U, s in a way that is significantly more efficient than the naive procedure.

The evaluation of $R(U, s)$ can be sketched diagrammatically as in Fig. 8. Unitaries outside the lightcones cancel in pairs with their daggered counterparts and two rhomboids of width $2t + 1$ sites remain. Considering only this part of the chain, and evaluating the diagram timestep by timestep, starting from ρ_0 in the middle, we encounter objects of dimension 4^{2t+1} .

After folding the daggered rhomboid upwards (Fig. 9), we can evaluate the folded rhomboids diagonally. This leads to a square root improvement, we encounter objects of dimension 2^{2t} . Note that this idea may be more generally applicable in tensor network contractions.

Owing to the single-site Haar invariance, the average of (84) remains the same when replacing all of the identities (“U-turns”) in the folded rhomboid diagram (Fig. 9)

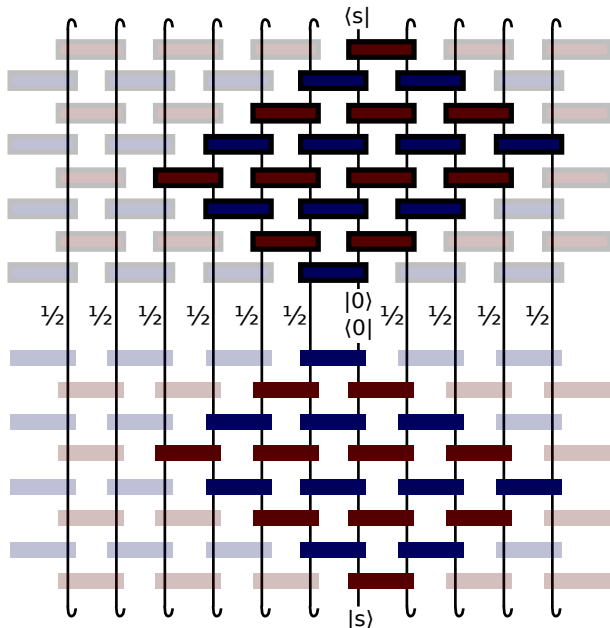


FIG. 8. Diagrammatic representation of (84) for $t = 4$. Unitaries outside of lightcones cancel and two rhomboids remain. A larger system results in more empty traces that do not contribute as they each have a factor $1/2$ attached. Sites are shown in the horizontal direction, unitaries U_i (V_i) are shown as blue (red) boxes. Their daggered counterparts lack a thick border.

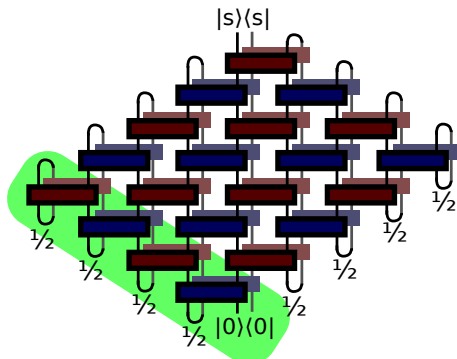


FIG. 9. The rhomboids from Fig. 8 can be folded above each other. The diagram is contracted diagonally, beginning with the shaded green part.

by $|0\rangle\langle 0|$. How this can be achieved is explained in detail in appendix C. We obtain two (disconnected) rhomboids that correspond to the absolute square of a single rhomboid as illustrated in Fig. 10. Again evaluating diagonally, we gain another square root as the objects only have dimension 2^t .

When sampling $\langle R(U, 0) \rangle_U$ according to the single-rhomboid method (Fig. 10) we observe a higher variance than using the folded-rhomboids procedure (Fig. 9). The data in Fig. 3 were compiled with the folded-rhomboids procedure only such that the strongly decreasing variance allows us to resolve the exponential decay of $\alpha(t)$.

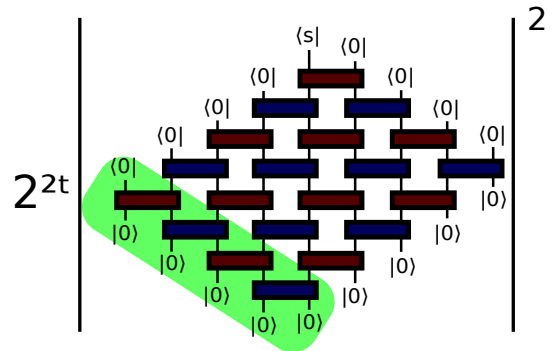


FIG. 10. The absolute value squared of a single rhomboid. The diagram is contracted diagonally starting with the shaded green part. After averaging the unitaries, this diagram has the same value as Fig. 9. See section V and appendix C for details.

The exponentially decreasing variance is also indicative of self-averaging of (84). To compile the data in Fig. 4, we want to access longer times and therefore make use of the single-rhomboid optimisation. To counteract the increasing variance, we use an importance sampling technique.

To perform importance sampling, we extend the random variable set to include s alongside $\{U_i\}, \{V_i\}$. Then we generate samples according to the probability distribution $R(U, s)$ with a Metropolis algorithm. Now note that $\langle R(U, 0) \rangle_U + \langle R(U, 1) \rangle_U = 1$ follows immediately from (84). Thus the normalization of the probability distribution $R(U, s)$ is trivial. The average value of δ_{s0} with respect to this probability distribution therefore results in $\langle R(U, 0) \rangle_U = (\alpha + 1)/2$.

The method presented here allows us to reduce the complexity of calculating the time evolution of t steps in a system of $2t+1$ sites (size of lightcone). Naively, time and space complexity both scale as 4^{2t+1} . Our simplifications give two square roots improvement, yielding a scaling of 2^t . Apart from the average over random unitaries, the numerical procedure is free of approximations.

The Monte Carlo aspect of the method can be generalized to improve the variance of expectation values $R_O = \langle \text{Tr}(O\psi_t) \rangle$ of arbitrary observables O over arbitrary ensembles of initial states or time evolutions determining ψ_t . Towards this end, extend s to a POVM including O instead of just $|0\rangle\langle 0|$ and $|1\rangle\langle 1|$ as for $R(U, s)$ above. Then perform Metropolis sampling of $\langle \text{Tr}(s\psi_t) \rangle$ with respect to the random variables determining ψ_t as well as s , which is taken as an additional random variable. Because of the normalization of the POVM, $\langle \delta_{sO} \rangle_{s, \psi_t} = R_O$.

VI. CONCLUSION AND OUTLOOK

In this paper, we have studied one dimensional particle chains under a random unitary time evolution operator

consisting of random nearest-neighbor gates. In spirit of Floquet evolution, the operator is repeated identically for subsequent timesteps.

We considered two cases, where the time evolution operator is a Gaussian circuit or consists of general unitaries. First, we were able to show strong results about the average evolution of chains of fermions under the Gaussian circuit time evolution. For Gaussian circuits inhomogeneous in space, we find that any initial state with vanishing two-point correlations at non-zero distances is simply scaled further towards the thermal mixture (11) and the initial two-point correlations can be recovered measuring expectation values; time evolution is localising. If the random time evolution operator is taken homogeneous in space, it delocalizes and leads to thermalization in the thermodynamic limit (12). We expect one can generalize our results to higher order correlation functions than the two-point functions studied in this work.

Next, we also considered spin chains under random unitary nearest-neighbor Floquet dynamics, inhomogeneous in space, with fixed finite local Hilbert space dimension. Our main result is (15): On a single site, the average evolution acts as a depolarising channel, completely independent of any other initial sites.

We employ new numerical methods (section V) to demonstrate that a time evolution composed of Haar distributed unitaries thermalizes. Under a different distribution with tunable random coupling strength, we find two regions of thermalization (strong coupling) and many-body localization (weak coupling), respectively.

As we have studied spins and fermions, it is natural to ask about a bosonic version of the problem. Since, contrary to fermions, each bosonic mode defines an infinite-dimensional Hilbert space, the generalization of Haar unitaries may pose mathematical problems. Nevertheless, for future work it is conceivable to work directly in the symplectic space (that corresponds to the covariance matrices) which is finite.

Both our analytical results as well as the numerical method can readily be generalized to higher dimensions. In the future, they may further also be applied to circuits with different topology and to Hamiltonian Floquet or stroboscopic dynamics with an ensemble of Hamiltonians having single-site Haar invariance.

ACKNOWLEDGMENTS

During preparation of this manuscript, related work [45] appeared on arXiv that provides evidence for an MBL transition in a different unitary circuit with random coupling strength.

This project has received funding from the European Research Council (ERC) under the European Union's Horizon 2020 research and innovation programme through the ERC Starting Grant WASCOSYS (No. 636201), the ERC Consolidator Grant GAPS

(No. 648913), and the ERC Advanced Grant QENOCOBA (No. 742102). D.P.G. acknowledges financial support of Severo Ochoa project SEV-2015-556 funded by MINECO.

Appendix A: Gaussian circuits: Uncoupled case

In this appendix, we calculate (54), which we repeat for convenience:

$$c(t\text{-avg}, k, N) = \frac{1}{4} \text{ for } \frac{2\pi}{N/2}k = 0, \pi, 2\pi.$$

For these values of k , \hat{G}_k is real and may be absorbed by the Haar-invariant transformation $Q \rightarrow \hat{G}_k^\dagger Q \hat{G}_k$ in (36). In turn, Q can be absorbed by the transformation $P \rightarrow Q^\dagger P$. Then we have simply $\hat{O}_k = P$.

This corresponds to two sites in the inhomogeneous uncoupled case where $Q_i = \mathbb{I}_4$ in the time evolution operator (4) and only P_i are independently random. We find much stronger localization (intuitively, information cannot spread) where the constant $c(t\text{-avg})$ is one quarter:

$$\langle \Gamma_{t\text{-avg}} \rangle = \frac{1}{4} \Gamma_0. \quad (\text{A1})$$

To show this it suffices to consider the first two sites $\Gamma_0^{1,2}$ and $P_1 \in O(4)$. We introduce an arbitrary $A \in O(4)$ by $P_1 \rightarrow AP_1A^\dagger$ using Haar invariance

$$\langle \Gamma_t^{1,2} \rangle = \langle AP_1^t A^\dagger \Gamma_0^{1,2} AP_1^{t\dagger} A^\dagger \rangle \quad (\text{A2})$$

and are free to integrate A over the orthogonal group. The integral can be evaluated [39] as

$$\langle \Gamma_t^{1,2} \rangle = \frac{1}{12} \langle (\text{Tr } P_1^t)^2 - (\text{Tr } P_1^{2t}) \rangle \Gamma_0^{1,2} \quad (\text{A3})$$

$$= \frac{1}{12} \left\langle \left(\sum_{i=1}^4 e^{i\beta_i t} \right)^2 - \sum_{i=1}^4 e^{i\beta_i 2t} \right\rangle \Gamma_0^{1,2}, \quad (\text{A4})$$

which is determined by the spectrum $\{e^{i\beta_i}, i = 1, 2, 3, 4\}$ of P_1 . We can evaluate this in the time average by observing that almost always

$$\beta_1 = -\beta_2, \beta_3 = -\beta_4 \text{ for } \det P_1 = +1 \quad (\text{A5})$$

and

$$\beta_1 = -\beta_2, \beta_3 = 0, \beta_4 = \pi \text{ for } \det P_1 = -1. \quad (\text{A6})$$

One can then show that in the time average of (A4), $\langle \cdot \rangle_{\det P_1 = +1} = 4 - 0$ and $\langle \cdot \rangle_{\det P_1 = -1} = 4 - 2$. Altogether the prefactor in (A3) matches the $1/4$ announced in (A1).

Appendix B: Spins: Uncoupled case

In this appendix, we find $\alpha(t)$ for the completely uncoupled probability distribution (16), the limit $h = 0$.

In that case, $U_i = u_{i,L} \otimes u_{i,R}$ and $V_i = v_{i,L} \otimes v_{i,R}$ are tensor products of single-site unitaries from the $U(2)$ Haar distribution. It then suffices to consider only one site $\rho_0 = \mathbb{I}_2/2 + \bar{\rho}_0$ as all sites are completely independent. Using the transformation $u \rightarrow v^\dagger u$, the v can be Haar-absorbed into the u , and we have the time evolution $\langle \rho_t \rangle = \langle u^\dagger \rho_0 u^{t\dagger} \rangle$ which we evaluate for general dimension of ρ_0 and u [43, 44].

By Haar invariance the transformation $u \rightarrow w^\dagger u w$ shows

$$\langle \rho_t \rangle = \langle w^\dagger u^\dagger w \rho_0 w^\dagger u^{t\dagger} w \rangle. \quad (\text{B1})$$

We can integrate out w with formula (62) and get the result

$$\langle \rho_t \rangle = \frac{\mathbb{I}_d}{d} + \frac{\lambda(t) - 1}{d^2 - 1} \bar{\rho}_0 \quad (\text{B2})$$

with the spectral form factor

$$\lambda(t) = \langle \text{Tr } u^t \text{Tr } u^{t\dagger} \rangle, \quad (\text{B3})$$

which is just (73) and (74) for a one-site chain and empty set I . For Haar-distributed $u \in U(d)$, the spectral form factor saturates at its maximal value $\lambda(t) = d$ for $t \geq d$ [46]. In particular, for our $d = 2$ chain and $t > 1$, $\lambda(t) = 2$ and the final state (15) stays constant with $\alpha = 1/3$.

Appendix C: Spins: Simplification for numerical calculations

In this section, we show that the computationally more efficient single rhomboid contraction in Fig. 10 is equiv-

alent to the function $R(U, s)$ from equation (84) when taking the average in U_i, V_i . This is needed in section V.

As argued in section V, $R(U, s)$ is equal to the folded rhomboids in Fig. 9. Let us consider each site (i.e. column) of that diagram in turn, apart from the central site containing s . The identities (“U-turns”) at the top and bottom of the column can be expanded. Linearity gives four new diagrams with all combinations of $|0\rangle\langle 0|$ and $|1\rangle\langle 1|$. Each column has either U_i or V_i both at the top and bottom. In the first case, single-site Haar invariance

$$U_i \rightarrow (w \otimes \mathbb{I}_2) U_i, V_i \rightarrow (\mathbb{I}_2 \otimes w^\dagger) V_i \quad (\text{C1})$$

allows to insert w and w^\dagger that cancel everywhere except at the very top. By choosing $w = \sigma_x$ the Pauli matrix, $|1\rangle\langle 1|$ at the top can be transformed into $|0\rangle\langle 0|$. This process can be repeated similarly to transform a $|1\rangle\langle 1|$ at the bottom into $|0\rangle\langle 0|$.

In total, applying this procedure at all sites results in 4^{2t} identical diagrams where all top and bottom parts are $|0\rangle\langle 0|$ (except for $|s\rangle\langle s|$). This only partially cancels with 2^{-2t} from the original bottom “U-turns”, giving the prefactor. The two rhomboids of unitaries and daggered counterparts are then disconnected and can be written as the absolute square of a single rhomboid.

-
- [1] Philip W Anderson, “Absence of diffusion in certain random lattices,” *Physical review* **109**, 1492 (1958).
 - [2] Michael Schreiber, Sean S Hodgman, Pranjal Bordia, Henrik P Lüschen, Mark H Fischer, Ronen Vosk, Ehud Altman, Ulrich Schneider, and Immanuel Bloch, “Observation of many-body localization of interacting fermions in a quasi-random optical lattice,” *Science* **349**, 842 (2015), arXiv:1501.05661.
 - [3] David A Huse, Rahul Nandkishore, and Vadim Oganesyan, “Phenomenology of fully many-body-localized systems,” *Physical Review B* **90**, 174202 (2014), arXiv:1408.4297.
 - [4] Dmitry A Abanin and Zlatko Papić, “Recent progress in many-body localization,” *Annalen der Physik* **529** (2017), arXiv:1705.09103.
 - [5] Günter Stolz, “Strategies in localization proofs for one-dimensional random Schrödinger operators,” in *Proceedings of the Indian Academy of Sciences-Mathematical Sciences*, Vol. 112 (Springer, 2002) pp. 229–243.
 - [6] Michael Aizenman and Stanislav Molchanov, “Localization at large disorder and at extreme energies: An elementary derivations,” *Communications in Mathematical Physics* **157**, 245–278 (1993).
 - [7] Jens H Bardarson, Frank Pollmann, and Joel E Moore, “Unbounded growth of entanglement in models of many-body localization,” *Physical review letters* **109**, 017202 (2012), arXiv:1202.5532.
 - [8] MC Bañuls, NY Yao, S Choi, MD Lukin, and JI Cirac, “Dynamics of quantum information in many-body localized systems,” *Physical Review B* **96**, 174201 (2017), arXiv:1707.05051.
 - [9] Marko Žnidarič, Tomaž Prosen, and Peter Prelovšek, “Many-body localization in the Heisenberg XXZ magnet in a random field,” *Physical Review B* **77**, 064426 (2008), arXiv:0706.2539.
 - [10] Eman Hamza, Alain Joye, and Günter Stolz, “Dynamical localization for unitary Anderson models,” *Mathematical Physics, Analysis and Geometry* **12**, 381 (2009), arXiv:0903.0028.
 - [11] Pedro Ponte, Z Papić, François Huveneers, and Dmitry A Abanin, “Many-body localization in periodically driven systems,” *Physical review letters* **114**, 140401 (2015), arXiv:1410.8518.
 - [12] Achilleas Lazarides, Arnab Das, and Roderich Moess-

- ner, “Fate of many-body localization under periodic driving,” *Physical review letters* **115**, 030402 (2015), arXiv:1410.3455.
- [13] Liangsheng Zhang, Vedika Khemani, and David A Huse, “A floquet model for the many-body localization transition,” *Physical Review B* **94**, 224202 (2016), arXiv:1609.00390.
- [14] C. W. von Keyserlingk, Tibor Rakovszky, Frank Pollmann, and S. L. Sondhi, “Operator hydrodynamics, otocs, and entanglement growth in systems without conservation laws,” *Phys. Rev. X* **8**, 021013 (2018), arXiv:1705.08910.
- [15] Tibor Rakovszky, Frank Pollmann, and CW von Keyserlingk, “Diffusive hydrodynamics of out-of-time-ordered correlators with charge conservation,” *Physical Review X* **8**, 031058 (2018).
- [16] Amos Chan, Andrea De Luca, and JT Chalker, “Solution of a minimal model for many-body quantum chaos,” arXiv preprint arXiv:1712.06836 (2017), arXiv:1712.06836.
- [17] Adam Nahum, Sagar Vijay, and Jeongwan Haah, “Operator spreading in random unitary circuits,” *Phys. Rev. X* **8**, 021014 (2018), arXiv:1705.08975.
- [18] Vedika Khemani, Ashvin Vishwanath, and David A. Huse, “Operator spreading and the emergence of dissipative hydrodynamics under unitary evolution with conservation laws,” *Phys. Rev. X* **8**, 031057 (2018), arXiv:1710.09835.
- [19] Adam Nahum, Jonathan Ruhman, Sagar Vijay, and Jeongwan Haah, “Quantum entanglement growth under random unitary dynamics,” *Physical Review X* **7**, 031016 (2017), arXiv:1608.06950.
- [20] Michael J Gullans and David A Huse, “Entanglement structure of current driven quantum many-body systems,” arXiv preprint arXiv:1804.00010 (2018), arXiv:1804.00010.
- [21] Tianci Zhou and Adam Nahum, “Emergent statistical mechanics of entanglement in random unitary circuits,” arXiv preprint arXiv:1804.09737 (2018), arXiv:1804.09737.
- [22] Joseph Emerson, Yaakov S Weinstein, Marcos Saraceno, Seth Lloyd, and David G Cory, “Pseudo-random unitary operators for quantum information processing,” *Science* **302**, 2098–2100 (2003).
- [23] Hrant Gharibyan, Masanori Hanada, Stephen H. Shenker, and Masaki Tezuka, “Onset of random matrix behavior in scrambling systems,” *Journal of High Energy Physics* **2018**, 124 (2018), arXiv:1803.08050.
- [24] Pavel Kos, Marko Ljubotina, and Tomaz Prosen, “Many-body quantum chaos: Analytic connection to random matrix theory,” *Physical Review X* **8**, 021062 (2018), arXiv:1712.02665.
- [25] Bruno Bertini, Pavel Kos, and Tomaz Prosen, “Exact spectral form factor in a minimal model of many-body quantum chaos,” arXiv preprint arXiv:1805.00931 (2018), arXiv:1805.00931.
- [26] Benoît Collins and Ion Nechita, “Random quantum channels i: graphical calculus and the Bell state phenomenon,” *Communications in Mathematical Physics* **297**, 345–370 (2010), arXiv:0905.2313.
- [27] PW Brouwer and CWJ Beenakker, “Diagrammatic method of integration over the unitary group, with applications to quantum transport in mesoscopic systems,” *Journal of Mathematical Physics* **37**, 4904–4934 (1996), arXiv:cond-mat/9604059.
- [28] Richard Jozsa and Akimasa Miyake, “Matchgates and classical simulation of quantum circuits,” in *Proceedings of the Royal Society of London A: Mathematical, Physical and Engineering Sciences*, Vol. 464 (The Royal Society, 2008) pp. 3089–3106, arXiv:0804.4050.
- [29] Sergey Bravyi, “Lagrangian representation for fermionic linear optics,” *Quantum Information & Computation* **5**, 216–238 (2005), arXiv:quant-ph/0404180.
- [30] This class includes (local) particle hole transformations. For example for a single fermionic mode, particle-hole transformation corresponds to the unitary $U = a + a^\dagger$ (a^\dagger/a creation/annihilation operators) and in the covariance matrix formalism, to $\begin{pmatrix} 1 & 0 \\ 0 & -1 \end{pmatrix} \in O(2)$ with negative determinant. All of the transformations we consider have definite parity as required by superselection rules.
- [31] Donald L Cohn, *Measure theory*, 2nd ed., Vol. 165 (Springer, New York, Heidelberg, 2003).
- [32] The Haar distribution will allow us to derive some analytical results. It treats all bases on an equal footing (this means there is no preferred local basis for the evolution), and rotation angles are random. It is also the most depolarising measure and thus one would expect to obtain the most extreme results. Physically, it corresponds to having magnetic fields not only with a random strength, but also a random direction.
- [33] Michael A. Nielsen and Isaac L. Chuang, *Quantum Computation and Quantum Information* (Cambridge University Press, Cambridge, 2000).
- [34] Rahul Nandkishore and David A Huse, “Many-body localization and thermalization in quantum statistical mechanics,” *Annu. Rev. Condens. Matter Phys.* **6**, 15–38 (2015), arXiv:1404.0686.
- [35] B Kraus and JI Cirac, “Optimal creation of entanglement using a two-qubit gate,” *Physical Review A* **63**, 062309 (2001), arXiv:quant-ph/0011050.
- [36] DM Basko, IL Aleiner, and BL Altshuler, “Metal-insulator transition in a weakly interacting many-electron system with localized single-particle states,” *Annals of physics* **321**, 1126–1205 (2006), arXiv:cond-mat/0506617.
- [37] Bela Bauer and Chetan Nayak, “Area laws in a many-body localized state and its implications for topological order,” *Journal of Statistical Mechanics: Theory and Experiment* **2013**, P09005 (2013), arXiv:1306.5753.
- [38] Jonas A Kjäll, Jens H Bardarson, and Frank Pollmann, “Many-body localization in a disordered quantum ising chain,” *Physical review letters* **113**, 107204 (2014), arXiv:1403.1568.
- [39] Benoît Collins and Sho Matsumoto, “On some properties of orthogonal Weingarten functions,” *Journal of Mathematical Physics* **50**, 113516 (2009), arXiv:0903.5143.
- [40] It is interesting to understand why the statement does not hold for $k = l$ and the two specific pairs. For $k = l$, it is obvious that $\hat{O}_k = \hat{O}_l$ are identical matrices and have identical spectra. The pairs $(k, l) = (N/2, N/4), (N/4, N/2)$ are the only values for which both \hat{G}_k and \hat{G}_l are real. As real orthogonal matrices, the eigenvalues of $\hat{O}_{k/l}$ are real (± 1) or arise as complex-conjugate pairs. In fact, for a quarter of all choices (P, Q) , the determinants are $\det \hat{O}_k = \det \hat{O}_l = -1$. These determinants force both matrices to both have an eigenvalue $+1$ and -1 .

- [41] Benoît Collins, “Moments and cumulants of polynomial random variables on unitary groups, the Itzykson-Zuber integral, and free probability,” *International Mathematics Research Notices* **2003**, 953–982 (2003), arXiv:math-ph/0205010.
- [42] Zak Webb, “The Clifford group forms a unitary 3-design,” arXiv preprint arXiv:1510.02769 (2015), arXiv:1510.02769.
- [43] Marko Žnidarič, Carlos Pineda, and Ignacio Garcia-Mata, “Non-Markovian behavior of small and large complex quantum systems,” *Physical review letters* **107**, 080404 (2011), arXiv:1104.5263.
- [44] Manuel Gessner and Heinz-Peter Breuer, “Generic features of the dynamics of complex open quantum systems: statistical approach based on averages over the unitary group,” *Physical Review E* **87**, 042128 (2013), arXiv:1301.1033.
- [45] Amos Chan, Andrea De Luca, and J. T. Chalker, “Spectral statistics in spatially extended chaotic quantum many-body systems,” *Phys. Rev. Lett.* **121**, 060601 (2018), arXiv:1803.03841.
- [46] Madan Lal Mehta, *Random matrices*, Vol. 142 (Elsevier, San Diego, 2004).
- [47] Alan Edelman and N Raj Rao, “Random matrix theory,” *Acta Numerica* **14**, 233–297 (2005).
- [48] J Ignacio Cirac, David Perez-Garcia, Norbert Schuch, and Frank Verstraete, “Matrix product unitaries: structure, symmetries, and topological invariants,” *Journal of Statistical Mechanics: Theory and Experiment* **2017**, 083105 (2017), arXiv:1703.09188.